SPATIAL AND TEMPORAL DISTRIBUTION OF DESICCATION CRACKS IN SHRINK-SWELL SOILS

A Dissertation

by

HALY LURY NEELY

Submitted to the Office of Graduate and Professional Studies of
Texas A&M University
in partial fulfillment of the requirements for the degree of

DOCTOR OF PHILOSOPHY

Chair of Committee,	Cristine L.S. Morgan
Committee Members,	Charles T. Hallmark
	Georgianne W. Moore
	James L. Heilman
Head of Department,	David D. Baltensperger

May 2014

Major Subject: Soil Science

ABSTRACT

Soil crack volume estimates, which are important for hydrology models on shrink-swell soils, are currently based on field measurements of vertical shrinkage and an assumption of isotropic shrinkage; however, few studies have validated the resulting crack volume estimates and studies have been limited to soils with very high shrink-swell potentials. In addition, the spatial variability of soil cracking potential is not well understood. First, I was able to improve *in situ* measurements of soil shrinkage by using a single borehole for all vertical soil movement and water content measurements. Then measurements of soil layer thickness and water content were made for seven soils with varying COLE values, from 0.01 to 0.17 m m^{-1}. Soil crack volume was estimated using cement slurry and photographing excavated soil layers at the end of the study. Over drying and wetting cycles, the relationship between soil layer thickness and water content was linear. Modifying an existing crack volume equation with shrink-swell potential and water content was a better fit to cement-estimated crack volume than the unmodified estimates, improving the r^2 from 0.06 to 0.84. The model over-predicted soil crack volume by a factor of 10 and a minimum shrinkage volume was required to generate visible soil crack volume. Finally, proximally-sensed bulk apparent electrical conductivity was highly correlated to inorganic C, and the depth of maximum sensitivity of the instrument was deeper than suggested by previous research in coarser textured soils. Because inorganic C is related to shrink-swell potential, it may be possible to use proximal sensors to map shrink-swell potential variability.

DEDICATION

For my father.

A God-fearing, George-Strait-loving, hard-working man.

ACKNOWLEDGEMENTS

I am grateful for the funding provided by the National Science Foundation (Grant No. EAR 0911317). I am also deeply grateful to my committee chair, Dr. Morgan, for her guidance and encouragement throughout this process. She has been instrumental in my development as a scientist. I would also like to thank my committee members, Dr. Hallmark, Dr. Moore and Dr. Heilman for their advice and support. Thank you also to my friends and colleagues in the Hydropedology group who are always there to help with field work or presentations, especially Dianna Bagnall and Liz Marley, who have been wonderful friends and colleagues, and Jason Ackerson, who challenged me to be a better scientist than I thought possible. Finally, I am grateful to my husband for his patience and support.

NOMENCLATURE

$\widehat{AVC}$	Estimated areal volume of cracks ($mm^3\ mm^{-2}$) using identified minimum shrinkage and modified slope
AVC	Areal volume of cracks ($mm^3\ mm^{-2}$)
AVC_{cement}	Areal volume of cracks estimated from photographs ($mm^3\ mm^{-2}$)
$AVC_{COLE,\theta}$	Areal volume of cracks predicted from COLE and θ ($mm^3\ mm^{-2}$)
AVC_L	Areal volume of cracks predicted from magnet data ($mm^3\ mm^{-2}$)
C	Carbon
COLE	Coefficient of linear extensibility ($m\ m^{-1}$)
e	Soil void ratio
EC_a	Bulk apparent electrical conductivity ($mS\ m^{-1}$)
EC_b	Electrical conductivity of the soil liquid phase
EC_s	Electrical conductivity of the soil solids
EC_w	Electrical conductivity of the soil solution
L	Measured length
L_0	Initial soil layer thickness, set at the beginning of the study period
L_{-1500}	Soil layer thickness at -1500 kPa water potential
L_{-33}	Soil layer thickness at -33 kPa water potential
$L_{COLE,\theta}$	Length as predicted from COLE and θ
L_{OD}	Length at oven dry
MBH	Multiple borehole analysis
NCSS	National Cooperative Soil Survey
NRCS	National Resource Conversation Service
RMSE	Root mean squared error

r_s	Dimensionless geometry factor
SBH	Single borehole analysis
T	Temperature (^oC)
USDA	United States Department of Agriculture
V	Volume
V_{-33}	Soil volume at -33 kPa water potential
V_{OD}	Soil volume at oven dry (105^oC)
V_s	Volume of soil solids
V_t	Total volume of soil
V_v	Volume of soil void space
z	One dimension
ΔL	Change in soil layer thickness
$\Delta L_{COLE,\theta}$	Change in length as predicted from COLE and θ, relative to initial conditions
ΔV	Change in volume
Δz	Change in one dimension (vertical)
θ	Volumetric water content ($m^3\ m^{-3}$)
θ_0	Initial volumetric water content, set at the beginning of the study period
θ_{-1500}	Volumetric water content at -1500 kPa water potential
θ_{-33}	Volumetric water content at -33 kPa water potential
θ_t	Volumetric water content at any point in time (t)

TABLE OF CONTENTS

Page

LIST OF FIGURES

FIGURE Page

FIGURE Page

LIST OF TABLES

CHAPTER I

INTRODUCTION AND LITERATURE REVIEW

Cracking soils and surface hydrology

Watershed management on landscapes with cracking clay soils is challenging due to uncertainty of soil crack volume and the temporal and spatial distribution of these soil cracks. As the soil loses water, large, vertical cracks open and preferentially route surface water into the subsoil (Fig. 1.1). However, if surface cracks are closed, soil hydraulic conductivity is significantly reduced and much of the precipitation can run off (Fig. 1.2) (Harmel et al., 2006). To improve surface hydrology models on shrink-swell soils, information of the spatial and temporal distribution of these cracks, and their volume, to correctly partition rainfall into runoff and infiltration is needed.

It may be possible to relate laboratory measurements of the potential of a soil to shrink and swell with water content to soil crack volume. Shrink-swell potential can be measured in the laboratory as the coefficient of linear extensibility (COLE, m m^{-1}), which is the length change of an intact soil ped between field capacity (-33 kPa) and oven dry (105^{o}C). The advantage of using COLE values to model soil cracking phenomenon is the database of these values provided by the Natural Resources Conservation Service (NRCS) as part of soil survey mapping. However, using COLE values from the NRCS soil surveys presents two concerns: 1) the coarse spatial scale of the available soil survey maps and 2) the lack of information of how to use COLE values to predict *in situ* soil cracking. To improve predictions of soil crack volume, I will

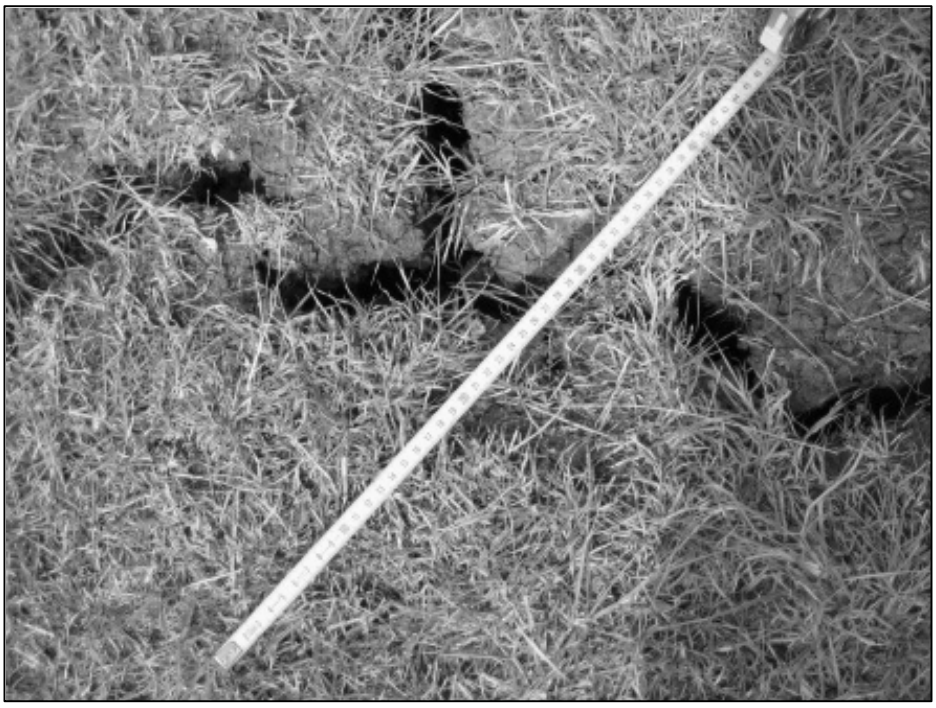

Figure 1.1. Desiccated soil with cracks present.

investigate possible methods to predict shrink-swell potential at scales finer than reported COLE values, and use field studies to define the relationship between COLE and *in situ* soil crack volume.

Spatial variability of some soil properties can be mapped at meter scale spatial resolution using electromagnetic induction, a common soil proximal sensing technique. Electromagnetic induction can be used to map soil properties that change the soil's electrical conductivity and has been shown to map salinity, clay content, soil water content (Rhoades et al., 1976; McBride et al., 1990; Corwin and Lesch, 2005; Brevik et al., 2006) and soil temperature (Robinson et al., 2009). Some of these properties also influence shrink-swell potential, suggesting the possibility of mapping shrink-swell

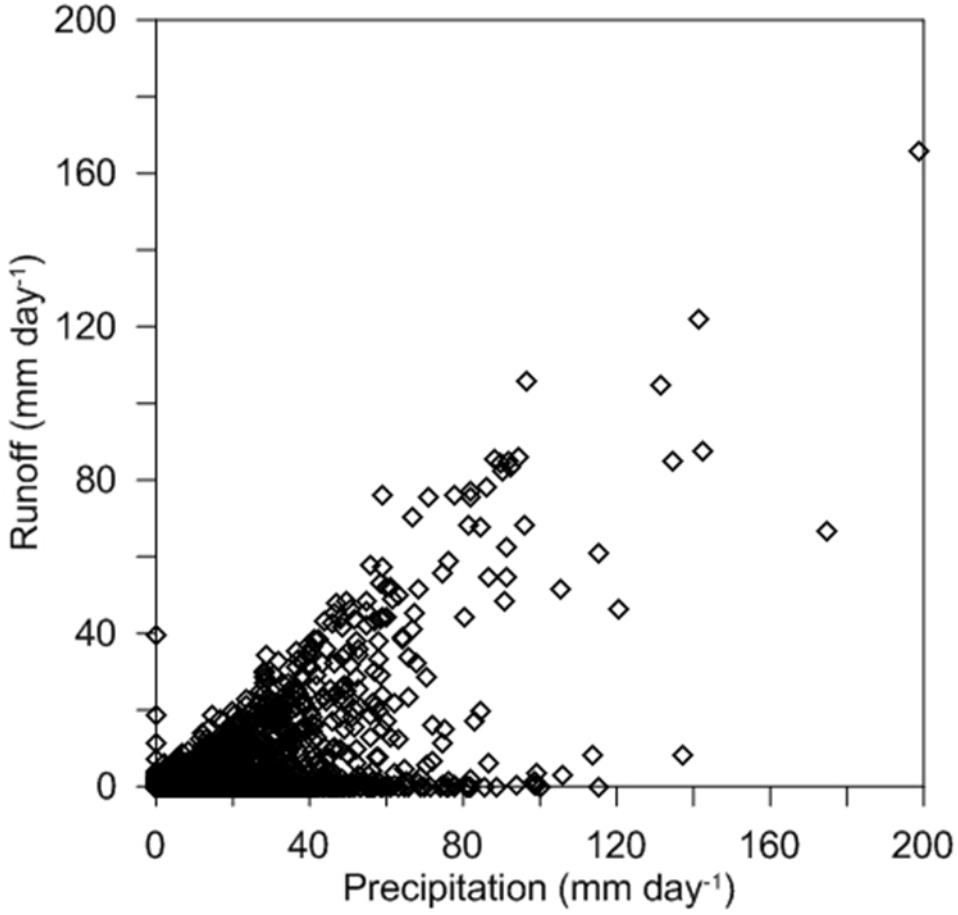

Figure 1.2. Precipitation and runoff in a Vertisol watershed (unpublished, Harmel).

potential at fine (1-10 m) scales. Identifying the variability of shrink-swell potential across landscapes could not only improve predictions of runoff across a landscape, but also improve site specific soil management by improving local predictions of soil water content.

Under laboratory conditions, individual soil peds often shrink isotropically. Current field-scale predictions of soil crack volume rely on translating one-dimensional

measurements to three-dimensional volume change through measuring vertical soil movement and assuming isotropic shrinkage (Aitchison and Holmes, 1953; Arnold et al., 2005) or applying a geometry factor obtained in a laboratory from individual peds (Bronswijk, 1990; Chertkov et al., 2004). However, when soil peds are organized into pedons *in situ*, some studies suggest the shrinkage behavior of the bulk soil does not behave like individual peds. As shrink-swell potential decreases, the vertical component begins to dominate which suggests a decrease in soil crack volume (Aitchison and Holmes, 1953; Cabidoche and Voltz, 1995) because the soil is preferentially shrinking vertically and not horizontally. Additionally, much of the literature focuses on high shrink-swell soils to the exclusion of low to medium shrink-swell soils. Moreover, there is little field validation in the literature of the accuracy of this assumption or studies comparing predicted vs. actual soil crack volume. To use laboratory measured shrink-swell potential to predict *in situ* crack volume, both measurements of vertical soil movement with soil water content over time and direct measurements of soil crack volume are necessary.

Favre et al. (1997) observed that localized soil swelling in response to increases in water content could complicate interpretations in soil shrinkage curves and identification of shrinkage geometries and subsequent cracking behavior. Field soil shrinkage with water content loss is commonly measured using individual soil anchors for each soil layer and a separate access tube for soil water content measured with a neutron moisture meter. Due to the sensitivity of the neutron moisture meter to the anchors and concrete and the need for each anchor to have its own location, these

measurements are made on separate volumes of soil (Arnold et al., 2005; Dinka et al., 2013). Shrink-swell soils often form with sub-meter scale subsurface variability called chimney-bowl features (Miller et al., 2010). These subsurface features are associated with surface gilgai microtopography, and fine-scale changes in soil properties such as clay content and inorganic C content (Wilding et al., 1989).

The specific objectives are to: 1) use proximal sensing to predict variability in shrink-swell potential in apparently uniform Vertisol landscapes; 2) develop methodology to reduce errors due to spatial variability associated with traditional soil thickness change measurements; and 3) measure the response of pedon thickness to changes in soil water content *in situ* and over a range of COLE values to define the relationship between COLE and the slope of field shrinkage curves; and 4) use COLE and direct measurements of soil crack volume to partition soil shrinkage into vertical and horizontal components.

Background

Spatial variability

The NRCS has developed and made available the Soil Survey Geographic (SSURGO) Database for almost every county in the United States, and soil scientists are working on developing a global database through the Digital Soil Mapping Project (McBratney et al., 2003). To scale up from pedons to polygons, the NRCS customarily delineates soil types along landscape positions and based on soil forming factors (Jenny, 1946; Schelling, 1970), despite the fact that soil properties may vary on finer spatial scales than landscapes (Cambardella et al., 1994). While many factors influence soil

cracking potential, including antecedent moisture content (Kishne et al., 2009), and land management practices (Wilding and Tessier, 1988), the primary soil properties are clay content and specific surface area of the clay particles (Franzmeier and Ross, 1968; Smith et al., 1985; Gray and Allbrook, 2002). Consequently, if COLE values are not available for a desired location, they can be estimated from other soil properties including clay content and mineralogy through a pedotransfer function (McBratney et al., 2002) e.g. Mbagwu and Abeh (1998) predicted volumetric soil shrinkage from organic matter content, clay content and cation exchange capacity in tropical soils.

In addition to shrink-swell potential, another feature of some Vertisols recognized by pedologists is the presence of gilgai. Paton (1974) described the microtopography termed 'gilgai' that occurs in some Vertisols. Gilgai, meaning small watering hole, are surface features that appear as small depressions with ridges in-between. Subsurface soil variations called chimney-bowl features (Miller et al., 2010) often coincide with surface topography and include increased clay content and organic carbon in the bowls/depressions and increased calcium carbonate in the chimneys/ridges. Long term studies of soil surface cracking patterns show the distribution and size of desiccation cracks are correlated to position on the gilgai surface, and large cracks often occur in the same location (Kishne et al., 2009).

Electrical conductivity and proximal soil sensing

Proximal sensing is a rapid, non-invasive method for mapping soil properties in the field, and can show variability at a finer scale than available in polygon soil maps. Bulk apparent soil electrical conductivity (EC_a) has been used extensively in mapping

zones of soil variability for precision agriculture (Lund et al., 1999; Johnson et al., 2001; Corwin and Lesch, 2005), and specific soil properties including salinity, clay content, soil water content (Rhoades et al., 1976; McBride et al., 1990; Corwin and Lesch, 2005; Brevik et al., 2006) and soil temperature (Robinson et al., 2009). The dominant soil properties are in descending order: salinity, soil water storage, and clay content. If a more dominant soil property is present, then a less dominant property cannot be mapped accurately (McBratney et al., 2005). Field maps created based on EC_a must always be corroborated with soil data (Carroll and Oliver, 2005).

In its simplest form, EC_a can be separated into two conductors:

$$EC_a = EC_b + EC_s \quad [1.1]$$

where EC_b is the liquid phase and EC_s is the surface conductivity of soil particles (Rhoades et al., 1976). By assuming electrical conductivity is related to water content by a linear relationship, EC_b can be partitioned and the relationship becomes

$$EC_a = EC_w*\theta*T + EC_s \quad [1.2]$$

where EC_w is the conductivity of the soil solution, θ is the volumetric water content, and T is the transmission coefficient. Furthermore,

$$T = \alpha*\theta + b \quad [1.3]$$

where α and b are fitting coefficients (Rhoades et al., 1976). Surface conductivity (EC_s) generally increases with increasing clay content and specific surface area of the clay particles and does not change with soil water content.

The soil properties that influence EC_a include salinity (Rhoades et al., 1976), water content (Kachanoski et al., 1990), clay content (Harvey and Morgan, 2009), and inorganic C (Kuhn et al., 2009), also correspond to gilgai microtopography in some Vertisols. The EM38 (Geonics, Canada) measures EC_a on a relatively small volume of soil (1 m^2 area, 1.5 m deep) (Rhoades and Corwin, 1981), which may be small enough to detect differences in landscapes with surface microtopography. Additionally, EC_a, as mapped by an EM38 in non-saline soils with uniform water content, should be correlated with clay content and specific surface area, both factors in identifying areas of shrink-swell potential. Factors such as an increase in inorganic C content should 'dilute' the clay content by decreasing the total specific surface area of the whole soil and therefore decrease the conductivity of the soil.

Geo-referenced EC_a data can be collected at much greater densities than direct methods such as soil cores (McBratney et al., 2005). Global positioning system antennas, such as the AgGPS (Trimble Navigation Limited, Sunnyvale, CA), coupled with a datalogger, allow rapid, geo-referenced EC_a data to be collected at high densities. This data can be spatially interpolated to produce soil maps at fine scales (1-10 m). It may be possible to use these interpolated maps to predict soil properties across

landscapes, as long as soil water content remains constant and interpolated maps have been verified with direct measurements (McBratney et al., 2005).

Laboratory soil volume changes

Soil shrinkage has been studied extensively in the laboratory, starting with Tempany (1917) and Haines (1923), who described soil volume change with change in water content. Haines (1923) identified three stages of the shrinkage curve: normal (water loss approximately equals volume loss, slope = 1), residual (more water is lost than volume, slope < 1) and zero (soil particle cannot move closer together, slope = 0). Stirk (1954) observed a fourth stage of structural shrinkage, where the ped loses water but not volume as water drains from the largest pores. Normal, or basic, shrinkage is generally the most common under field soil water conditions, and is assumed to be a 1:3 ratio vertical change to volume of water lost (Aitchison and Holmes, 1953; Yule and Ritchie, 1980; Arnold et al., 2005).

COLE (m m^{-1}) is expressed as a relative change in volume by

$$\mathrm{COLE} = \frac{V_m^{1/3} - V_d^{1/3}}{V_d^{1/3}}, \qquad [1.4]$$

where V_m is the total volume of the soil at field capacity, commonly set at -33 kPa, and V_d is the volume of the soil when oven dried to 105ºC. Regardless of the shrinkage geometry in the laboratory, COLE is expressed as a change in one-dimension only (m m^{-1}). The total volume of the soil can be expressed as

$$V_t = V_s + V_v = V_s + e \cdot V_s = V_s \cdot (1 + e) \quad [1.5]$$

where V_t is the total volume of the soil, V_s is the volume of the solids, V_v is the volume of voids and e is the void ratio. I can now modify the COLE equation to just the change in void space. If shrinkage is isotropic, then

$$z = V_t^{1/3} \quad [1.6]$$

where z is the change in length in any direction.

Johnston and Hill (1945) compared shrinkage curves from natural clods of Austin and Houston Black clays, and found that Houston Black did not display structural shrinkage but Austin clay did. The authors attribute this difference to the draining of large voids in the Austin clay. It is interesting to note that these two clay soils had very different shrinkage curves, and entered shrinkage stages at different water contents. Consequently, a range of COLE values and soils should be studied to gain an accurate picture of soil shrinkage behavior.

Soil subsidence is a vertical-only measurement and was related to volume change in Bronswijk (1989) by

$$1 - \frac{\Delta V}{V} = \left(1 - \frac{\Delta z}{z}\right)^{r_s} \quad [1.7]$$

where V is the initial volume, z is vertical height, and r_s is a dimensionless factor. For soils with only vertical shrinkage, $r_s = 1$, and with isotropic shrinkage $r_s = 3$. Bronswijk (1990) found in the laboratory under loads similar to subsoil conditions, most soils exhibited an r_s value close to 3, suggesting that the entire soil pedon may experience isotropic shrinkage. However, this study was done with single peds, and may not be an accurate representation of how soil peds behave when organized into a whole soil pedon.

Field soil subsidence (vertical soil movement)

Translating soil shrinkage into predictions of soil crack volume is generally done by monitoring changes in vertical soil movement, and the assumption of isotropic shrinkage (Aitchison and Holmes, 1953; Arnold et al., 2005) or a geometry factor (Bronswijk, 1990; Chertkov et al., 2004). Field subsidence measurements are often made by installing soil anchors, and monitoring the elevation change over time (Coquet et al., 1998; Arnold et al., 2005; Dinka et al., 2013). An additional access tube for moisture content is installed to relate water loss to elevation loss. To calculate soil crack volume, the elevation change in one direction (vertical) is assumed to be a third of the total volume change, and the remaining volume change is assigned to crack volume. This assumption is based on the fact that soil peds often shrink isotropically in the laboratory. However, these are theoretically or experimentally derived parameters and not easily developed for a watershed or landscape, and there is little field validation of predicted vs. actual soil crack volume.

However, there is evidence that when soil peds are organized into pedons the slope of the shrinkage curves change, and not to the same degree for all soils (Aitchison and Holmes, 1953; Cabidoche and Voltz, 1995). Field soil shrinkage has been observed as slightly less than normal (1:1, equal soil volume loss to volume of water loss), and may be attributed to layers in the soil undergoing residual shrinkage (Aitchison and Holmes, 1953; Cabidoche and Ruy, 2001). Cabidoche and Voltz (1995) saw anisotropic shrinkage and suggested the soil shrank vertically more than horizontally. Possible explanations include a more pronounced effect of residual shrinkage within soil layers, the presence of horizontal cracks, or a difference in soil mineralogy. COLE values were not reported in these studies, but the presence of cracks was indicated in the text.

This uncertainty in the stages of shrinkage *in situ* pedons experience, and the partitioning of vertical and horizontal shrinkage, demonstrates the need for field verification by directly measuring soil crack volume before an accurate model can be built. Favre et al. (1997) observed that localized soil swelling along edges of soil peds and crack faces, making the shrink-swell process in pedons highly spatially variable. Any field shrinkage curve methodology that introduces spatial variability may affect the slope of the curve, and any predictions of soil crack volume using those curves.

Measurements of *in situ* soil crack volume over time have been done with fluid filled bags inserted into cracks (Stewart et al., 2012) or linear gauges fastened to facing sides of a soil crack (Favre et al., 1997). However, these methods involve measuring individual cracks, and may influence soil crack behavior and propagation. Other

methods for soil crack volume measurement include direct filling with sand (Dasog and Shashidhara, 1993) and liquid latex (Abou Najm et al., 2010).

CHAPTER II

INSTRUMENTATION TO MEASURE SOIL SUBSIDENCE AND WATER CONTENT IN A SINGLE BOREHOLE: A TECHNICAL NOTE

Introduction

In soils that shrink and swell, a loss of soil water decreases the total volume of the soil, and re-wetting increases the volume. In soils with high shrink-swell potentials, e.g. Vertisols and Vertic intergrades, soil shrinkage also results in the formation of large, vertically-oriented cracks capable of capturing surface runoff. The volume of these desiccation cracks has been estimated by measuring the change in soil layer thickness, or alternatively, by the measuring or modeling the change in soil water content coupled with the knowledge of the relationship between soil shrinkage and water content (Bronswijk, 1991). Field measurements of soil shrinkage with loss of water can be derived from measurements made in separate boreholes (Woodruff, 1937; Arnold et al., 2005; Dinka et al., 2013), but this method makes defining the relationship between soil shrinkage and water content problematic due to unknown effects of spatial variability in the shrink-swell process. Additionally, current methods employed to directly measure soil shrinkage are tedious and lack precision for looking at individual subsoil layers. This paper introduces methodology that allows soil shrinkage and water content measurements to be made in a single borehole, creating opportunity for detailed study of the relationship between vertical shrinkage and water loss. The goal of this methodology was to reduce uncertainty in the relationship between soil layer thickness

and water content by 1) eliminating horizontal variability in the measurements, 2) increasing precision of vertical measurements, 3) decreasing site disturbance during installation and subsequent measurements, and 4) reducing the tedious nature of field measurements.

Vertical movement of soil has been monitored by measuring the change in elevation between subsoil anchors and a deeply anchored reference (Woodruff, 1937; Arnold et al., 2005; Dinka et al, 2013) or the soil surface (Hallaire, 1987; Coquet, 1998). Anchors that have been used include cement footings (Arnold et al., 2005; Dinka et al., 2013), screws (Coquet, 1998), and metal plates (Woodruff, 1937), and are typically placed at the bottom of a borehole. Rods extending from the anchor to a convenient height above the soil surface are used to monitor movement of the anchors. Since placing multiple anchors at the same horizontal location in the soil (i.e., in the same borehole) presents some technical difficulties, measurements of vertical movements, and of soil water content associated with the vertical movements, have usually been made at separate, but closely spaced locations (Cabidoche and Voltz, 1995). As previously mentioned, a major limitation to these anchor-based methods arises from spatial variability associated with measurements made at different horizontal locations. With such measurements the relationship of thickness to water content is often unclear (Fig. 2.1).

Spatial variability in shrink-swell behavior is due to two not wholly independent phenomena: 1) variation in physical and chemical properties of soil (Wilding et al., 1989) and 2) variation in the distribution of soil water (Towner, 1968; Cabidoche and

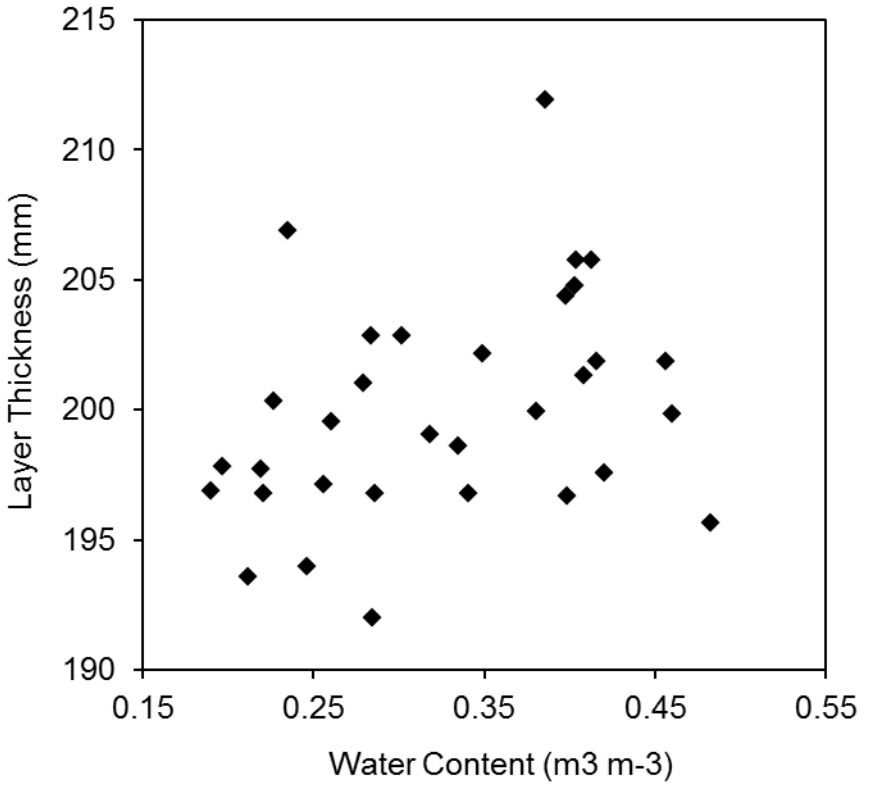

Figure 2.1. Relationship between thickness and water content of a nominally 20-cm thick layer of Houston Black clay soil as determined from changes in elevation of concrete anchors placed at the bottom of separate 20- and 40-cm deep boreholes and from water content measured in a third borehole (data unpublished).

Voltz, 1995). Shrink-swell soils with gilgai often display a high degree of meter and submeter spatial variability in shrink-swell potential, water holding capacity, cracking behavior, and other morphological and physical properties (Wilding et al., 1989). These variations can occur over distances appreciably less than the practical spacing of the location of shrinkage and water content measurements. Shrinkage also varies with

landscape position on a hillslope to watershed scale due to variation of surface hydrology and variation in the shrink-swell potential of the soil (Baer and Anderson, 1997). To overcome some of the difficulties arising from horizontal variability in shrinkage and swelling, I developed a method based on the co-locating of shrink-swell and water content measurements in a single borehole.

Instrumentation

Materials for the single borehole method included small magnets, a custom-made device to insert the magnets into the sidewall of the borehole, a track-based, magnetic field sensor linked to a datalogger, and a neutron moisture meter (InstroTek, Inc., Raleigh, NC, Model 503DR1.5). Although the measurements and data processing were all done in SI units, the instrumentation was built using English units because of the materials and equipment available. Both units will be presented. To use this system, first a 5.1-cm (2 inch) borehole was vertically augered into the soil. Magnets were then inserted into the borehole wall at desired depths. When all the magnets were installed, a thin-walled, 5.1-cm diameter PVC tube (schedule 20, AirVac, Model VM101-8, ASTM F2158-8) was inserted into the borehole to maintain access. As the soil shrinks and swells, the magnets changed position relative to the soil surface, and by resolving the location of the magnets I could measure changes in the thicknesses of the soil layers bound by any pairs of magnets. During measurements, a magnetic field sensor was propelled by a screw drive down the hole and voltage changes resulting from changes in the direction of each magnetic ‘s flux field as it was passed were recorded on the datalogger. The distance the sensors travel down the hole was determined by counting

the revolutions of the screw-drive using combined a magnet fixed to the revolving drive and a stationary magnetic field sensor. Soil moisture was recorded with the neutron moisture meter in the same access tube.

Magnets

Neodymium magnets (KJ Magnetics, D3X0, axially magnetized) were selected for their strength of magnetic field compared to traditional ferrite magnets. Cylindrical magnets, 0.48 cm in diameter by 2.54-cm long (3/16 by 1 inch), were encased in aluminum sleeves to increase area of contact with the soil (Fig. 2.2C) and minimize the possibility of magnets falling down cracks. The sleeves were made from 0.64-cm thick bar stock, and cut to 1.75 by 2.54 cm (1/4 by 11/16 by 1 inch).

Magnet inserter

The magnet inserter (originally designed by Anthony Mantalbano (AM Machine Shop, Bryan, TX) and strengthened by Doug Tucker (Hydraulics Works Inc., Bryan, TX)) used a 0.95-cm (3/8-inch) diameter, 60° V-threaded rod with a thread spacing of 0.16 cm to push 0.95-cm (3/8-inch) diameter ball bearings (Fig. 2.2A), a bronze (SAE 660) push plate (Fig. 2.2B), and the magnet in a sleeve (Fig. 2.2C) along a track (Fig. 2.2D) and into the soil. The push plate allowed the magnet to be pushed slightly past flush with the borehole wall to ensure successful installation, and had wire threaded through it to allow the push plate to be retracted from the soil after magnet insertion by pulling on the wire at the soil surface. Bronze was used for the push plate because it self-lubricated. The material for the threaded drive rod (4140 chromium molybdenum steel) was chosen for its stiffness. The main body for the magnet inserter was machined

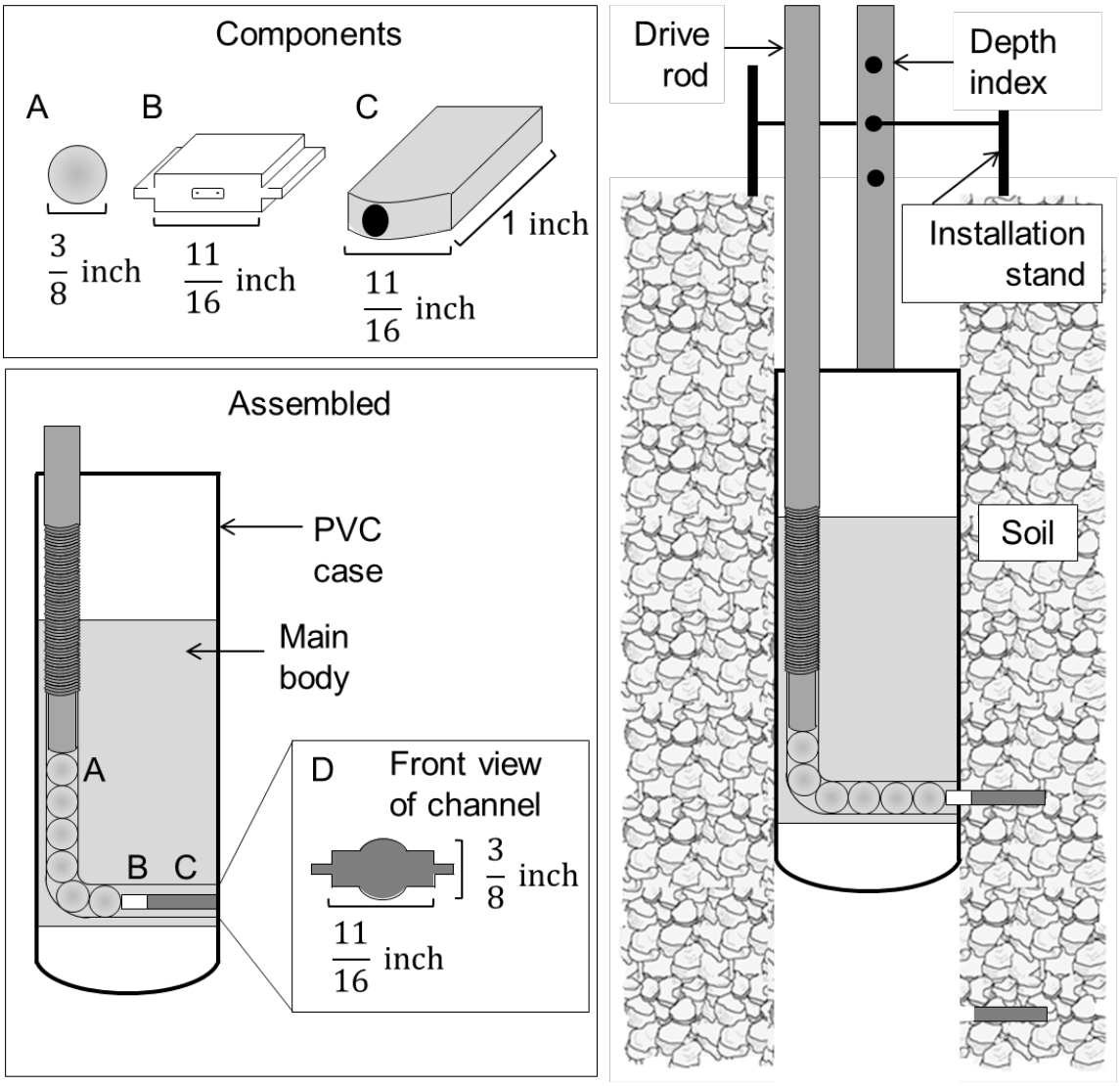

Figure 2.2. Diagram for magnet inserter. Components include A) ball bearings, B) push plate, C) aluminum-sleeved magnet, and D) front view of magnet inserter channel. A threaded drive rod is used to generate the necessary force to move components and push the magnets into the soil, and magnet position from the soil surface is set with a depth indexed rod with an installation stand.

from a round bar of 1045 carbon steel and had a cover made of the same PVC pipe type used for soil moisture access tubes, and was the same outer diameter as the augered hole (5.1 cm or 2 inches). The magnet inserter was then mounted to a 2.54-cm wide (1 inch)

aluminum angle track that was used to index installation depths relative to the soil surface. The index-rod with the inserter attached is then suspended over the borehole using an installation stand. The corners of the magnet sleeves were shaved to match the contour of the cylindrical face of the PVC-covered body of the inserter so as not to protrude and drag along the side of the borehole while the magnet-loaded inserter was being lowered into the borehole.

Magnet position sensor

The magnet position sensor for locating the position of each magnet was constructed using three magnetoresistive sensors (HMC 1501, Honeywell, Plymouth, MN), an aluminum angle track, and a motor-rotated, threaded rod (Fig. 2.3). This same sensor was used to count rotations of a magnet attached to the screw-drive rod (0.95-cm (3/8-inch) diameter, 60° V-threaded rod with a thread spacing of 0.16 cm) to determine distance of the sensor assembly from the soil surface in the borehole. The HMC 1501 chips sensed the direction of the magnetic flux, providing an accurate location of the magnets than a field-strength sensor. Outputs from all magnetoresistive sensors were logged on a CR23X datalogger (Campbell Scientific, Logan, UT) and the data were processed using Matlab R2012a (The MathWorks, Inc., Natick, MA).

Three aspects of this system make it advantageous to other systems currently in use: 1) soil movement and moisture measurements are made on the same of soil surrounding a borehole; 2) the thickness change of individual soil layers can be measured more precisely; and 3) the footprint of the measurement system is small to minimize soil disturbance for subsequent soil crack measurements.

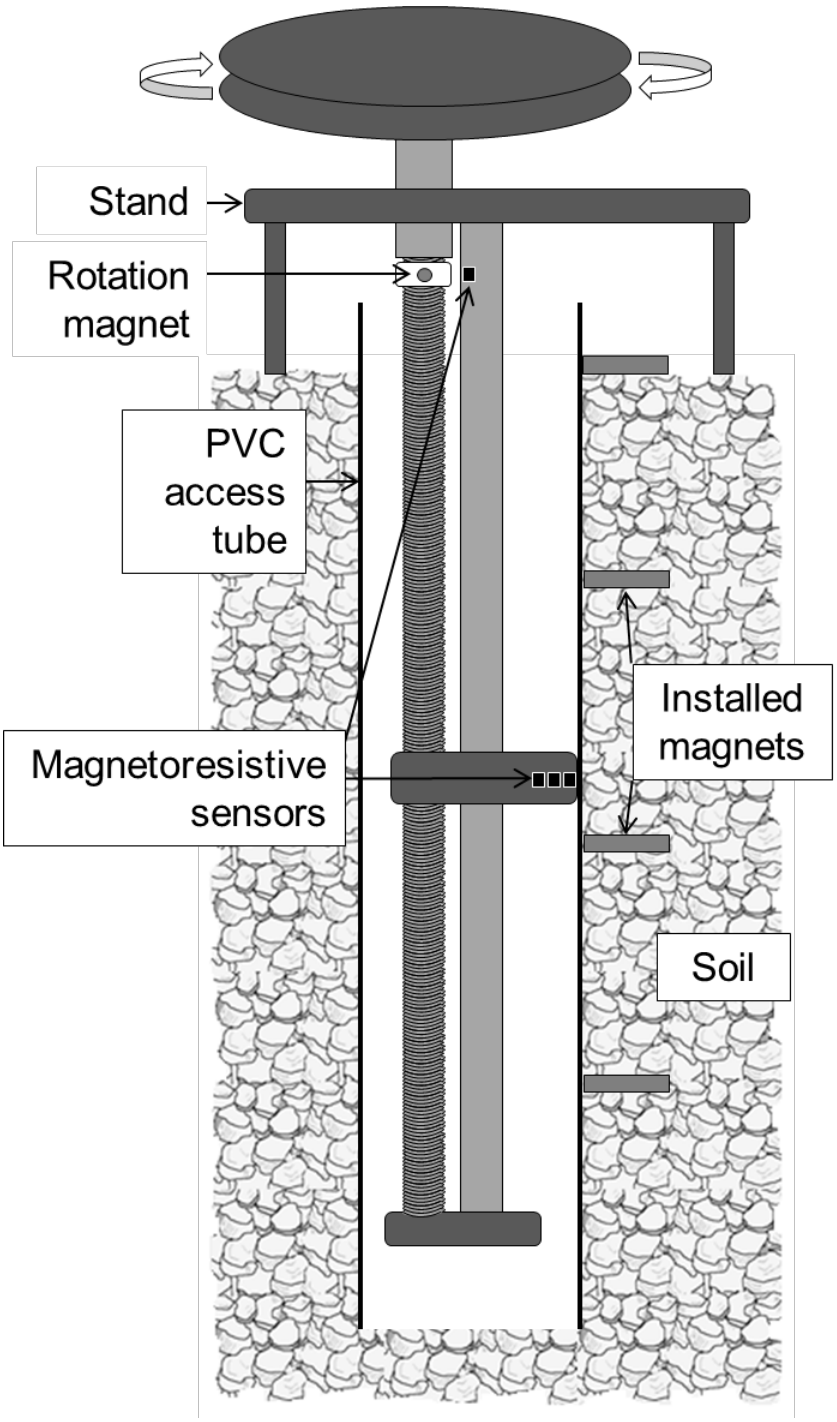

Figure 2.3. The magnet sensor instrument scans magnet position relative to the soil surface by moving magnetoresistive sensors down the borehole. To measure magnet depth, an additional magnetoresistive sensor counts rotations of the threaded rod.

Materials and methods

Soils/site selection

To test the measurement system, two sites were selected based on shrink-swell potential and clay mineralogy. Soils at both sites were Vertisols- Burleson clay (fine, smectitic, thermic Udic Haplustert) and Ships clay (very-fine, mixed, active, thermic Chromic Hapluderts). The mean coefficients of linear extensibility (COLE) were 0.11 and 0.15 m m^{-1} for soils at the Burleson clay and Ships clay sites, respectively. Both sites were near College Station, TX (30°36′05″N 96°18′52″W) and used for pasture.

Installation

In preliminary testing, I found that the installation of magnets into the borehole wall was easier when the soil was moist than when dry. For this reason, the two sites, 3 by 3 m, were first irrigated and then covered with plastic sheeting to minimize evapotranspiration during redistribution. At each site, four 5.1-cm boreholes were augered vertically to a depth of 1.5 m at the vertices of a 2-m square. The magnet inserter, mounted to a depth-indexed stand, was then lowered down the borehole, and magnets were installed at 10, 20, 40, 60, 80, and 100 cm from the soil surface. A PVC tube was inserted after magnet installation to maintain the integrity of the access for subsequent measurements. Prior to taking measurements to locate the magnets in the borehole, a magnet was placed at the soil surface adjacent to the outer edge of the PVC pipe to reference the position of the soil surface.

Soil water content was measured at 5, 10, 15, 30, 50, 70, and 90 cm below the soil surface in the borehole using the neutron moisture meter and a depth-control stand

(Evett et al., 2003). Additional calibration for surface measurements is needed to account for neutrons escaping to the atmosphere when measurements are taken close to the soil surface (Evett et al., 2006); one option is to use correction factors, which scale the surface measurements so a single calibration equation can be used (Grant, 1975). Under uniform soil water conditions, correction factors for surface measurements were estimated by minimizing the difference between expected and observed count ratios for each measurement depth. Any observed decrease in count ratio was assumed to be the influence of the surface. A single calibration equation was then developed using the corrected surface and unmodified subsurface count ratios and soil water content measurements. The resulting calibration equation was linear with an r^2 of 0.87 and RMSE of 0.026 $m^3\ m^{-3}$. Volumetric water content measurements were interpolated with depth using a cubic spline, and then averaged over each soil layer using the positions of the magnets that measurement day.

Measurement timing

Measurement dates were from 27 July 2012 to 4 Oct. 2012, a total of 70 d. Two dry-down periods, both beginning at close to field capacity, were devised by controlling soil water content with greenhouse plastic and irrigation. Plots were kept dry during rain events with high-light transmission greenhouse plastic installed 0.5 m from the soil surface to allow air circulation. I removed the plastic covers when there was a low probability of rain; however, it rained briefly on August 17 and 19 (study days 22 and 24) without plastic covers. Rain events recorded at a weather station approximately 6 km away were approximately 2 and 1 cm for those two day, respectively; however, there

was only evidence of precipitation at the sites on August 19. To re-wet plots during the study, plots were irrigated on August 9, 11 and 14 (study days 14, 16, and 19) using spray-head sprinklers at an intensity of 3 cm h^{-1}. Both soils received 3 to 4 cm of water during each irrigation event; water was applied until ponding was observed and then allowed to infiltrate to reduce surface runoff. All measurements of soil layer thickness, calculated as magnet position relative to the previous magnet, and volumetric water content means are relative to the beginning of the study.

Results and discussion

Measurement precision

The precision, or repeatability, of the magnet position sensor was assessed using three repeated measurements within the same borehole. The magnet position sensor could resolve the location of an installed magnet to the nearest 0.33 mm. In comparison, elevation change of soil anchors has been measured to the nearest 3 mm with a laser level (Arnold et al., 2005) and systems using linear displacement transducers can measure changes of 5 μm (Coquet et al., 1998). Standard deviation of magnet position relative to the soil surface and the thickness of individual soil layers tended to increase with increasing depth (Table 2.1), with a mean standard deviation for all soil layers of 0.5 mm. This standard deviation was reasonable considering the magnets were 4.8 mm in diameter. Standard deviation was comparable to that of a laser level used to measure elevation of rods attached to anchors in the soil (A Sz. Kishne, personal communication, 2013). This sub-millimeter repeatability of individual soil layers provides the opportunity to measure soil shrink-swell on a finer spatial scale, both vertically and

Table 2.1. Mean position, standard deviation, and bias for three repeated measurements of magnet position.

	Soil layer number					
	1	2	3	4	5	6
	Magnet position relative to the soil surface (mm)					
Mean	84.4	184.6	382.7	583.3	785.3	984.7
Standard deviation	0.57	0.42	0.27	0.27	0.72	0.98
Bias (x 10^{-14})	-1.4	-2.8	5.7	0.11	0.11	-0.11
	Magnet position relative to previous magnet (mm)					
Mean	84.4	100.1	198.1	200.7	202.0	199.3
Standard deviation	0.57	0.16	0.31	0.00	0.94	0.82
Bias (x 10^{-14})	-1.4	-2.8	0	0	2.8	0

horizontally, and temporal scale than traditional methods currently allow.

Field shrinkage measurements

Measurements of soil shrink-swell with the magnet position sensor were precise enough to observe mm-scale changes in soil layer thicknesses over short time periods. An additional benefit of the magnet-based measurements is that the magnet position sensor can be operated by a single person, whereas laser leveling requires two individuals to be practical. Measurements of water content and magnet position for a single borehole can be made in approximately 15 minutes.

Change in soil layer thickness and water content, referenced to the initial conditions, followed similar trends over time for both sites (Fig. 2.4). The behavior of three soil layers (0 to 20, 40 to 60, and 80 to 100 cm) is similar for the remaining soil

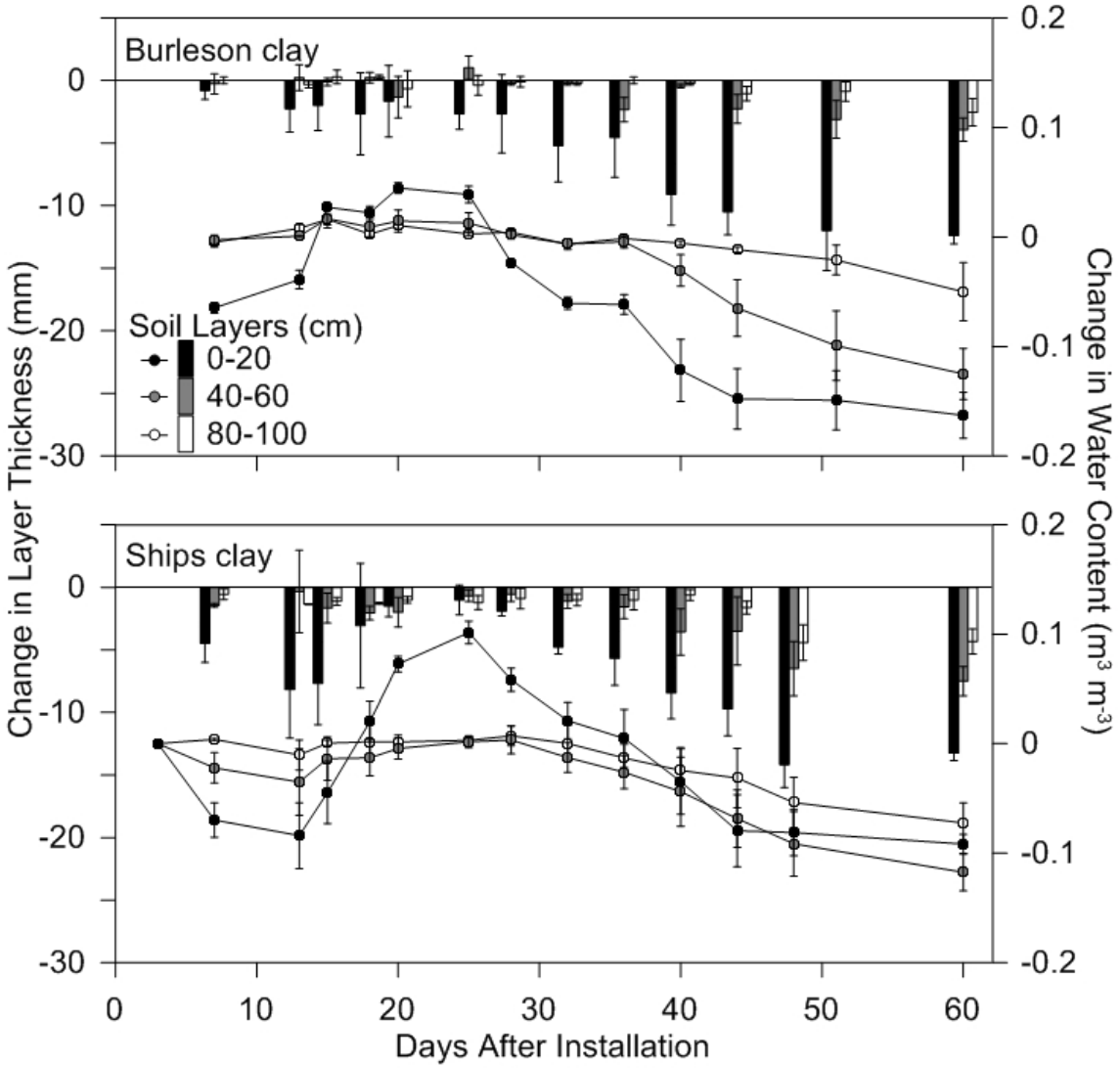

Figure 2.4. Change in layer thickness (bars) and water content (circles and lines), referenced to initial conditions, of three layers over time for Burleson clay and Ships clay. Bars represent one standard deviation from the mean.

layers, which are not shown. Generally, change in layer thickness decreased over time until the irrigation events. The surface layer for both sites had the greatest observed spatial variability, with mean standard deviation of soil layer thickness of the 4 locations

for Burleson clay and Ships clay of 2.26 and 1.96 mm, respectively. Mean standard deviation tended to decrease with increasing depth; the 40 to 60-cm and 80 to 100-cm layers had mean standard deviations of 0.78 and 0.53 mm for Burleson clay, and 1.30 and 0.55 mm for Ships clay.

For both sites, the standard deviation of soil shrink-swell for all layers ranged from 1 to 4 mm across all measurement days. There was more observed heterogeneity in the shrink-swell process as the soil rewetted as compared to the end of the study period (Fig. 2.4). Given that the precision of layer thickness measurement was less than 1 mm, it is likely these observations were primarily the result of natural spatial variability rather than instrument error during wetting events. Interestingly, standard deviation of soil water content was lowest during rewetting, so the variability in layer thickness cannot be explained by heterogeneity at the scale which soil water was measured. The variability of change in water content was highest when the soil was drying, with standard deviation maximums of 0.03 $m^3\ m^{-3}$ and 0.07 $m^3\ m^{-3}$ for Burleson clay and Ships clay, respectively. Standard deviation of three repeated measurements of water content in a single borehole were less than 0.001 $m^3\ m^{-3}$, or about 0.2 mm of water for a 20-cm soil layer, under both wet and dry soil conditions. Even though measurements made over time are likely less precise due to air gaps that form as the soil shrinks away from the access tube (Jarvis and Leeds-Harrison, 1987), it is likely there was meter-scale variability in soil water content.

The relationship between change in layer thickness and change in soil water content was generally linear and highly correlated for the three presented layers in both

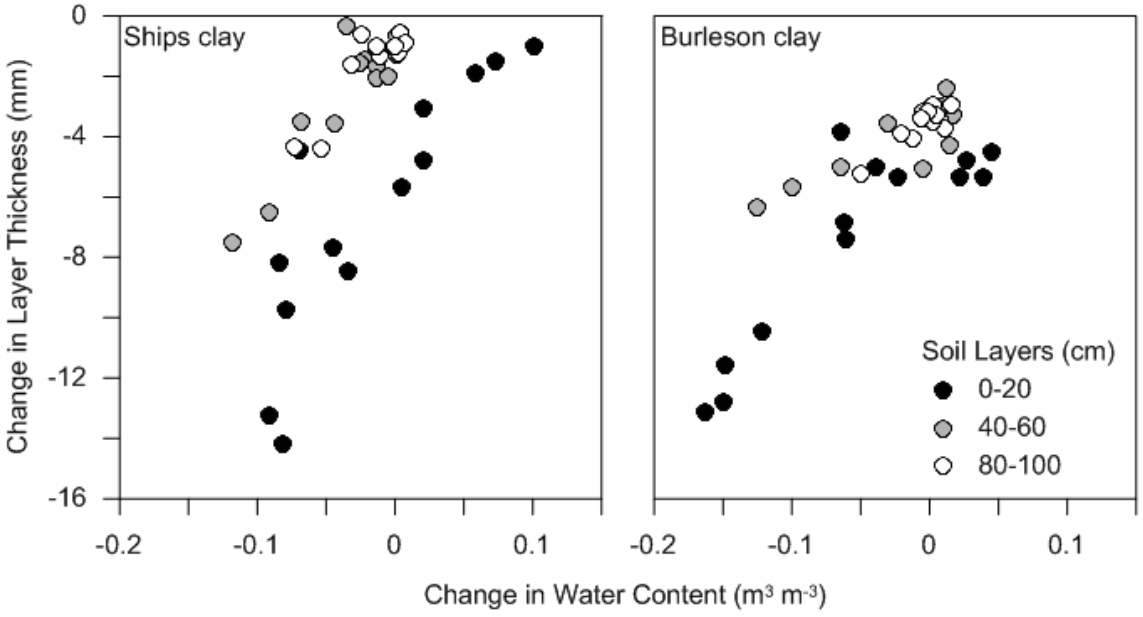

Figure 2.5. Change in soil layer thickness with change in water content, referenced to initial conditions, for the two sites. Data for the three soil layers are site means.

sites (Fig. 2.5) as well as the remaining layers. For the Burleson clay, r^2 values of 0.90, 0.88, and 0.90 were observed for the three soil layers (0 to 20, 40 to 60, and 80 to 100 cm) of the Burleson clay, and 0.82, 0.92, and 0.87 for Ships clay. The Burleson clay had less subsoil shrinkage than the Ships clay despite a similar decrease in soil water content. These differences in subsoil shrinkage are likely due to the 0.04 m m^{-1} difference in COLE, or shrink-swell potential, between the sites.

Single vs. multiple borehole analysis

To evaluate the effect of spatial variability on *in situ* field shrinkage curves, I compared soil shrinkage and water content from a single borehole to the same relationship using data from multiple boreholes (Fig. 2.6). For each site, one layer was

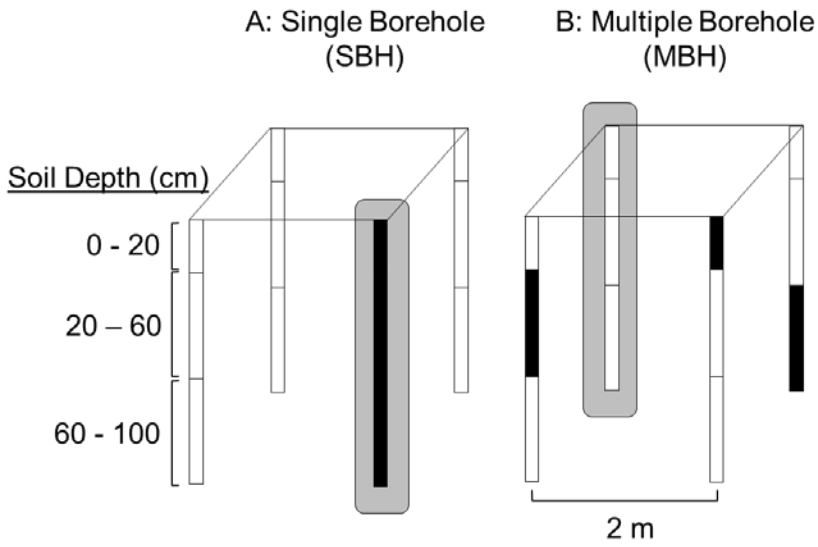

Figure 2.6. Single borehole (A) vs. multiple borehole (B) analysis, using boreholes installed on the vertices of a 2-m square at one site. Black sections represent layer thicknesses for the three soil layers and gray shading shows the positions for water content measurements.

used from each of the boreholes and combined to form a single profile, and water content was measured from the fourth and separate borehole. The resulting correlation was compared with the correlations observed using all layers and soil water content from a single borehole. The multiple borehole analysis in this study was similar to some current methods of field measurements of soil shrinkage with individual soil anchors for each layer and a separate borehole for soil water content. Correlations between shrinkage and soil water loss were improved when all measurements were from a single bore-hole, r^2 improved from 0.73 to 0.90 for both sites (Fig. 2.7). This analysis addresses differences in layer thickness between boreholes, but it does not address differences in shrinkage of soil below the measurements zones at the locations, which can be an appreciable source of error (Dinka et al, 2013). I did not measure

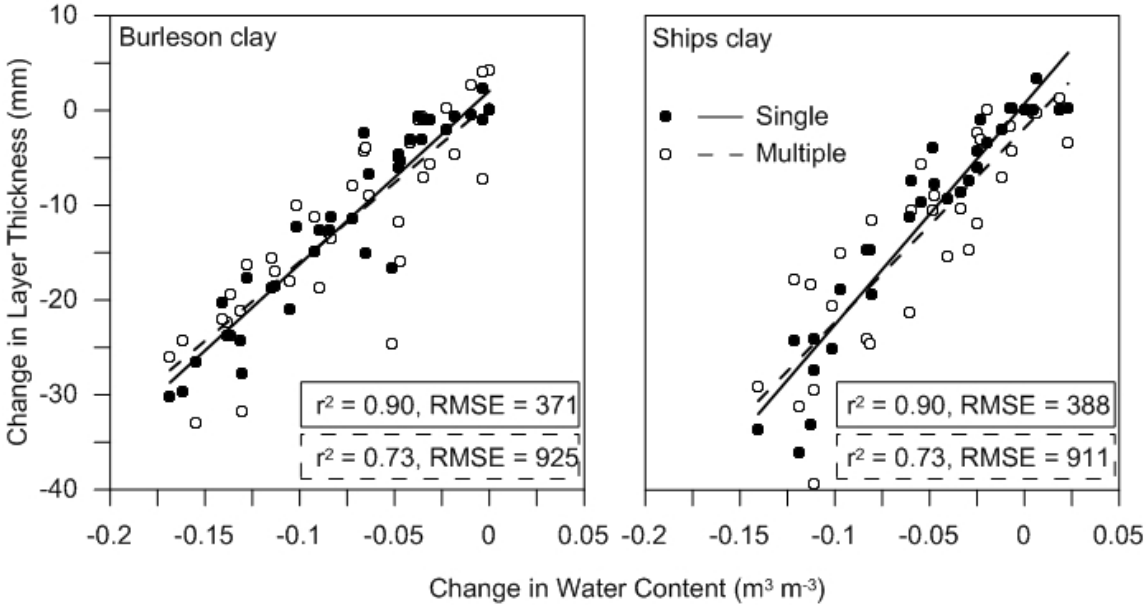

Figure 2.7. Change in layer thickness vs. change in water content, referenced to initial conditions, for Ships clay and Burleson clay for the upper meter of soil. Closed black circles and solid lines represent single borehole analysis (SBH), and open circles and dotted lines represent multiple borehole analysis (MBH).

differences in elevation of the surface magnets between boreholes and cannot address this issue. For this reason, it was possible that I underestimated the true improvement of the new method using this simulation, but these results did illustrate the spatial variability in the shrink-swell process at the meter to submeter scales.

Separate borehole measurement systems often cannot observe trends unless under strong drying conditions (Kirby et al., 2003), and/or cannot observe shrink-swell processes of individual subsurface soil layers (Dinka et al., 2013). Horizontal spatial variability in the shrink-swell process likely accounts for some of these difficulties.

Conclusions

This technique for measuring *is situ* soil subsidence offers several proven advantages over previous methods including:

1. More accurate relationships between soil water loss and soil shrink-swell due to the elimination of horizontal variability;
2. Many soil layers can be measured simultaneously and with improved accuracy compared to anchor methods;
3. Streamlined and rapid installation with a lower degree of soil disturbance and;
4. Measurements can be made by one person and in less than 15 min per borehole.

With this improved method, researchers will be able to make more measurements with higher accuracy of *in situ* soil shrink-swell behavior. This method will provide higher quality data on *in situ* soil shrinkage providing valuable information on the behavior of shrink-swell soils and aid our understanding of the hydrology and genesis of Vertisols and Vertic intergrades.

CHAPTER III

MODELING SOIL CRACK VOLUME AT THE FIELD SCALE USING AVAILABLE SOIL DATA

Introduction

In soil profiles, unreliable predictions of infiltration and redistribution of water are partially due to preferential flow pathways created by soil structure, cleavage planes, root channels, animal burrows, and other discontinuities in the soil matrix (Beven and Germann, 1982). In shrink-swell soils, preferential flow also occurs in the large, vertical desiccation cracks that form under dry soil conditions, but few studies have measured the depth or volume of these cracks, especially at the pedon scale. The presence and extent of desiccation cracks are both important pieces of information because these cracks are capable of capturing large amounts of surface runoff; however, when the soil is moist and the cracks are closed, these soils have low infiltration rates. The uncertainty of the volume and geometry of these soil cracks, and the specific conditions for crack opening, are major causes of inaccurate simulations of runoff and infiltration by current hydrology models (Harmel et al., 2006). The ability to know where on the landscape the cracks are occurring, what their volumes are, and when they open is necessary for partitioning rainfall into surface runoff and infiltration on landscapes that contain shrink-swell soils.

Current methods to predict soil crack volume include measurements of vertical soil movement with the assumption of isotropic shrinkage (Aitchison and Holmes, 1953;

Arnold et al., 2005) and use laboratory-developed geometry factors (Bronswijk 1990; Chertkov et al., 2004). Because laboratory measurements of soil ped shrinkage show individual soil peds shrink isotropically, soil scientists have used this knowledge to predict soil crack volume from changes in the vertical thickness of an *in situ* soil profile (Arnold et al., 2005; Bronswijk, 1990). However, there is little field validation in the literature of the resulting crack volume predicted using vertical shrinkage and assumptions of isotropy. Measuring vertical changes in soil profile thickness is time and labor intensive, and these measurements are often not validated with direct measurements of *in situ* soil crack volume (Rivera, 2011) or linked to a soil property so that the information can be translated to another soil or location. In this manuscript, field measurements of vertical profile movement, soil water content, and crack volume are measured and linked to a measureable soil property, the shrink-swell potential, or the coefficient of linear extensibility (COLE).

Shrink-swell soils gain and lose volume with increasing and decreasing soil water content, respectively, and the change in ped shape is isotropic. Many laboratory studies have quantified the change in volume of an individual soil ped with losses in water content, called a soil shrinkage curve, and was first described by Tempany (1917) and Haines (1923). Haines (1923) identified three stages of the shrinkage curve: normal or basic (water loss approximately equals volume loss, slope = 1), residual (more water is lost than volume, slope < 1) and zero (soil particle cannot move closer together, slope = 0). Stirk (1954) observed a fourth stage called structural shrinkage, where the ped loses water but not volume as water drains from the largest pores. However, when

Johnston and Hill (1945) compared the shrinkage curves of soil peds from two clay soils, the soil with the lower clay content exhibited structural shrinkage while the higher clay content soil did not. The shape of the shrinkage curve of an individual ped depends on distribution of pore sizes, clay content, specific surface area of soil particles, and other physical and structural properties (Chertkov, 2007).

There is evidence that the shrinkage behavior of a pedon of intact soil is different from an individual ped (Cabidoche and Voltz, 1995; Yule and Ritchie, 1980). Unlike the multiple shrinkage stages of individual peds, the relationship between soil shrinkage and water loss under field conditions has been shown to be linear (Aitchison and Holmes, 1953; Dinka et al., 2013). No evidence for structural shrinkage of intact pedons has been attributed to soil layers undergoing basic and residual shrinkage simultaneously (Aitchison and Holmes, 1953; Cabidoche and Ruy, 2001; Cabidoche and Voltz, 1995). Additionally, in a laboratory study, the slope of the shrinkage curve of intact soil cores was less than slopes of individual peds (Crescimanno and Provenzano, 1999). If the slope and shape of field shrinkage curves are different from laboratory measurements, then using laboratory-derived assumptions to calculate soil crack volume from vertical subsidence is unsuitable. Uncertainty of *in situ* soil shrinkage phenomena supports the need for field verification by directly measuring soil shrinkage and soil crack volume.

At the ped-scale, soil shrink-swell potential is measured in the laboratory as COLE, which is the length change of a ped between field capacity and oven dry. Yule and Ritchie (1980) observed a linear relationship between the vertical shrinkage of 5-cm diameter soil cores and the COLE values of those cores, suggesting COLE can be used

to model *in situ* soil shrinkage. Lepore et al. (2009) used COLE and descriptions of soil structure provided by the NRCS soil survey to parameterize a two-domain mesopore and matrix (M&M) model of water infiltration and redistribution. The widths of the mesopores are controlled by soil water content and COLE, with wider mesopores developing under lower water contents. Using a similar approach, it may be possible to use COLE to parameterize models predicting soil crack volume.

Because soil properties vary across landscapes, building models that describe soil behavior and that are based on soil properties that are measureable, or are already available in databases, ensures utility of the model. Naturally occurring spatial variability in soil properties makes it important to use field measurements to calibrate or parameterize an entire watershed or landscape (Lepore et al., 2009). The advantage of using COLE values in a soil crack volume model is that COLE is measured for each horizon of every soil series that exhibits Vertic properties, and published by the NRCS national gridded soil database (gSSURGO; Soil Survey Staff, 2014). While factors other than the shrink-swell potential influence soil cracking, including antecedent moisture content (Kishne et al., 2009), land management practices (Wilding and Tessier, 1988), and vegetation (Mitchell and van Genuchten, 1992), the COLE value is the potential for a soil to change volume with changes in water, which is largely a function of clay content and specific surface area of the clay particles (Gray and Allbrook, 2002). Consequently, if COLE values are not available for a desired location, they may be estimated using pedotransfer functions and other soil properties including clay content and mineralogy (Wilke, 2010). The disadvantage of using COLE values is the disparity

between the shrinkage behavior of a fist-sized ped compared to a connected pedon of soil within the soil fabric across a landscape. To use the NRCS database, first knowledge of ped shrinkage must be translated into shrinkage and cracking behavior of an *in situ* soil pedon.

The overall goal of this research was to develop a mechanistic model to estimate soil crack volume using measurable soil properties and soil water content. To achieve this, models for soil layer thickness and crack volume, using knowledge of ped shrinkage and soil properties, were developed and compared with *in situ* measurements of soil layer thickness and water content in seven soils possessing a range of COLE values. At the end of 10 weeks of drying, sites with surface cracks were filled with a cement slurry and excavated to estimate soil crack volume.

Methods and materials

Site selection

To investigate how COLE affects *in situ* soil shrinkage curves and crack volume, seven soils with a range of COLE values from almost zero to 0.17 m m^{-1} (Table 3.1) were selected. All study sites were near College Station, TX (30°36′05″N, 96°18′52″W), and under perennial grass and forbes vegetation. At each study site, a 3- by 3-m plot was established to measure soil shrink-swell and water content over time. Sites were brought close to field capacity before installing the measurement system by thoroughly wetting the soil and allowing 2 weeks for redistribution. During the 2 weeks, sites were covered by black plastic to reduce evapotranspiration and achieve a relatively uniform soil water content with depth. Then four 5.1-cm boreholes were augured

Table 3.1. USDA-NRCS classification of each soil.

Soil texture	COLE (m m^{-1})	NRCS soil series	Taxonomic class
Very fine sandy loam	0.01	Yahola fine sandy loam	coarse-loamy, mixed, superactive, calcareous, thermic Udic Ustifluvents
Silt loam	0.03	Weswood silt loam	fine-silty, mixed, superactive, thermic Udifluventic Haplustepts
Silty clay loam	0.06	Weswood silty clay loam	fine-silty, mixed, superactive, thermic Udifluventic Haplustepts
Sandy clay loam	0.08	Unidentified	
Clay	0.11	Burleson clay variant	fine, smectitic, thermic Udic Haplusterts
Clay	0.14	Ships clay	very-fine, mixed, active, thermic Chromic Hapluderts
Clay	0.17	Burleson clay	fine, smectitic, thermic Udic Haplusterts

vertically to a depth of 1.5 m at the vertices of a 2-m square and the magnets and access tubes were installed.

Shrink-swell measurements

In situ soil shrink-swell and water content measurements were co-located in a single borehole (Chapter II). Materials for the single borehole method include small magnets, a custom-made device to insert the magnets into the sidewall of the borehole, a track-based, magnetic field sensor linked to a CR23X datalogger (Campbell Scientific, Logan, UT), and a neutron moisture meter (InstroTek, Inc., Raleigh, NC, Model 503DR1.5). Cylindrical magnets (0.48 by 2.54 cm) were encased in rectangular

aluminum sleeves (0.64 by 1.75 by 2.54 cm) to increase the surface area and maintain soil contact. The inserter, mounted to a depth-indexed stand, was dropped down the open hole and used to install the aluminum-encased magnets at 10, 20, 40, 60, 80, and 100 cm from the soil surface, with an additional magnet placed at the soil surface during measurements. A thin-walled PVC access tube was placed in the hole after magnet installation.

To take measurements, the magnetic field sensor was propelled down the access tube and the installed magnets induce a change in voltage which was recorded by the datalogger. The magnets were located using the voltage output, and the distance sensors travel down the hole was recorded using an additional magnetic field sensor with a rotating magnet. Sensor responses were collected on a CR23X datalogger (Campbell Scientific, Logan, UT). The magnetic-field-sensor could resolve the position of the installed magnets to 0.33 mm, with repeatability of less than 1 mm. Data analysis was done in Matlab R2012a (The MathWorks, Inc., Natick, MA). Soil layer thickness (L) was calculated by subtracting each magnet location from the previous magnet. Change in layer thickness (ΔL) was defined as the relative change from study day 1, i.e. the initial layer thickness (L_0).

Water content profile measurements

After each measurement of magnet position, soil water content was measured at 5, 10, 15, 30, 50, 70, and 90 cm depths from the soil surface using a neutron moisture meter and a depth-control stand (Evett et al., 2003). The neutron moisture meter was field-calibrated in PVC access tubes for three soil types. Surface measurements of soil

water content with the neutron moisture meter needed additional calibration to account for neutrons escaping to the atmosphere (Evett et al., 2006). A single calibration equation was used by scaling the surface measurements following the method of Grant (1975). Under uniform soil water conditions, correction factors for surface measurements were calculated by minimizing the difference between expected and observed count ratios for surface measurements, where observed decreases in count ratios at the surface were assumed to be due to lost neutrons. Soil-specific calibration equations, using the surface corrections, were used to convert neutron count ratios to soil water content. The calibrations were linear relationships between volumetric water content and count ratio with the following r^2 and root mean squared error (RMSE) values: fine sandy loam (0.37, 0.020 $m^3\ m^{-3}$), silt loam and silty clay loam (0.67, 0.032 $m^3\ m^{-3}$), and all three clay sites (0.86, 0.027 $m^3\ m^{-3}$). Soil water content measurements for each measurement day were interpolated with depth using a spline function, and then integrated for each soil layer using magnet positions for that measurement day in Matlab R2012a (The MathWorks, Inc., Natick, MA) to account for soil shrinkage. Change in water content ($\Delta\theta$) was defined as the relative change in soil water content from study day 1, i.e. the initial water content (θ_0).

Measurement timing

Soil layer thickness and water content were measured from 27 July 2012 to 4 October 2012, a total of 70 days. Two dry-downs were measured in this time period. To re-wet plots during the study, plots were irrigated on August 9, 11 and 14 (study days 14, 16, and 19) using spray-head sprinklers. Water was applied until ponding was observed

and then allowed to infiltrate. Plots were protected from rain with high-light transmission greenhouse plastic installed 0.5 m from the soil surface to allow air circulation, and covers were removed when there was a low probability of rain.

Crack volume estimates

At the end of 70 days, and when all sites were sufficiently dry, three sites had visible surface cracks and were filled with 1:1 (by volume) slurry of water and Type 1 white Portland cement. Dish soap was added as an air entrainer in a 1:300 ratio of dish soap to cement slurry to weaken the cement for easier excavation. Plots were excavated in layers parallel to the soil surface at approximately 5, 15, 30, 50, 70, and 90 cm. High resolution digital photographs were used to estimate soil crack volume for each layer. A fixed grid of colored pins was installed on the soil layer surface for each soil layer and was used as control points to correct photographs for possible uneven soil surfaces and edge effects and to order the photographs into a single image for each soil layer. An individual photograph covered approximately 0.6 by 1 m of the soil surface, and each pixel represented a 0.04-mm^2 area.

The resulting photographs of cracking patterns for the whole plot were converted to black and white images, with cracks as white pixels. White pixels were counted within a 1-m radius from an access tube, and then using pixel size and layer thickness, converted to soil crack volume, accounting for plot edges. This radius was chosen because it was representative of the crack density for each access tube. Image processing was done in Matlab R2012a and Photoshop (Adobe Photoshop CS6, San Jose, CA).

Model theory and assumptions: soil layer thickness

The laboratory measurement of the shrink-swell potential of a soil ped, COLE, is calculated as the change in volume of an individual soil ped between field capacity (-33 kPa) and oven dry (< -1500 kPa), relative to the oven dry volume. Our first assumption was that an individual soil ped will shrink isotropically, and therefore the length change, or change in one dimension, is the cube root of the volume change. The COLE value therefore was the change in length of an intact soil ped relative to the dry length, defined as

$$\mathrm{COLE} = \frac{V_{-33}^{1/3} - V_{OD}^{1/3}}{V_{OD}^{1/3}} = \frac{L_{-33} - L_{OD}}{L_{OD}}, \qquad [3.1]$$

where V_{-33} and V_{OD} are the volumes of the soil ped at -33 kPa and oven dry (OD) respectively; similarly, L_{-33} and L_{OD} represent the cube root of volume, or linear dimension of a soil unit. Because COLE is based on a measurement of an individual soil ped, COLE does not directly account for changes in inter-pedal volume. Additionally, soil peds were allowed to equilibrate at these water potentials before volume measurements were taken, and I would not expect soil peds to reach equilibrium under the heterogeneous drying conditions of *in situ* soil layers at the pedon scale.

Next, I assumed the slope of the shrinkage curve is linear for a soil layer at field moisture conditions, which has been observed in previous studies (Cabidoche and Ruy,

2001; Crescimanno and Provenzano, 1999). The linear slope for a field soil shrinkage curve becomes,

$$\text{slope} = \frac{L_{-33} - L_{-1500}}{\theta_{-33} - \theta_{-1500}}, \quad [3.2]$$

which is the slope between field capacity (-33 kPa) and permanent wilting point (-1500 kPa). If the slope of the relationship between field soil shrinkage with water content is linear, soil layer thickness and soil water content at field capacity (L_{-33}, θ_{-33}) may be substituted with initial conditions of soil water content and layer thickness (L_0, θ_0),

$$\text{slope} = \frac{L_0 - L_{-1500}}{\theta_0 - \theta_{-1500}}. \quad [3.3]$$

Using the first day of observations is useful for model development purposes because field capacity would rarely or infrequently be experienced in a field experiment. In addition, wilting point water content (θ_{-1500}) is available in the NRCS database.

To complete the slope term (Eq. [3.3]), I solved for layer thickness at permanent wilting point (L_{-1500}) using COLE (Eq. [3.1]). I assume that soil layer thickness at θ_{-1500} and θ_{OD} were sufficiently similar, and that this substitution would not significantly modify the slope in Eq. [3.3]. By rearranging Eq. [3.1], I can solve for layer thickness at permanent wilting point (L_{-1500}),

$$L_{-1500} = L_0\left(\frac{1}{COLE + 1}\right). \quad [3.4]$$

Using the modified slope (Eq. [3.3]) and change in water content, I can predict change in layer thickness as

$$\Delta L_{COLE,\theta} = \frac{L_0 * (1 - \frac{1}{COLE + 1})}{\theta_0 - \theta_{-1500}} * (\theta_0 - \theta_t). \quad [3.5]$$

Change in layer thickness ($\Delta L_{COLE,\theta}$) is a function of COLE and volumetric water content (θ) at any points in time (θ_t). Now that the change in layer thickness is mathematically defined, crack volume can be estimated assuming isotropic shrinkage.

Model theory and assumptions: crack volume

To evaluate the effectiveness of using COLE in the prediction of soil cracking, the following three independent calculations of the crack volume were compared: 1) crack volume as a function of change in soil layer thickness measured from magnet positions (Bronswijk, 1989), 2) crack volume as a function of measurements of water content and COLE (based on Eq. [3.5], and 3) crack volume estimated using photographs of cement-filled cracks. The first and second estimates are the Bronswijk approximation and our modified Bronswijk approximation. The Bronswijk approximation (Bronswijk, 1989) predicts the areal volume of cracks (AVC, $m^3\ m^{-2}$), or the volume of cracks per unit area, based on vertical soil shrinkage, using the equation

$$\mathrm{AVC} = \left(1 - \left(1 - \frac{L_1 - L_2}{L_1}\right)^{r_s}\right) * L_1, \quad [3.6]$$

where L_1 is the layer thickness before soil shrinking or swelling, and L_2 is layer thickness after. A dimensionless geometry factor, r_s, is the proportion of shrinkage in the vertical and horizontal directions. An r_s factor of 3 is isotropic shrinkage, less than 3 implies more vertical than horizontal shrinkage, and more than 3 is more horizontal than vertical shrinkage. I continued the assumption of isotropic shrinkage in calculating AVC (AVC_L) from initial layer thickness (L_0) and subsequent change layer thicknesses (ΔL) as measured from magnet positions, so that

$$\mathrm{AVC_L} = \left(1 - \left(1 - \frac{\Delta L}{L_0}\right)^3\right) * L_0. \quad [3.7]$$

To model AVC from water content and COLE, I substituted modeled change in layer thickness from water content and COLE for ΔL in the Bronswijk approximation for a new model of soil crack volume, or the modified Bronswijk approximation,

$$\mathrm{AVC_{COLE,\theta}} = \left(1 - \left(1 - \frac{\left(1 - \frac{1}{\mathrm{COLE} + 1}\right)}{\theta_0 - \theta_{-1500}} * (\theta_0 - \theta_t)\right)^3\right) * L_0. \quad [3.8]$$

Our third calculation of AVC came from direct measurements of cracks filled with cement calculated from photographs. Cement-estimated soil crack volume (AVC_{cement}), AVC_L, and $AVC_{COLE,\theta}$ were independent estimates of soil crack volume on the same volume of soil and were used to assess both the Bronswijk and the modified Bronswijk approximations.

Results and discussion

The mean water contents and soil layer thicknesses from each access tube for each soil layer and study day were plotted. The relationship between change in water content and change in soil layer thickness for the upper meter of soil was linear for all soils in this study. To test linearity, the residuals of a linear fit were plotted with fitted values and all residuals were homoscedastic. As well, the r^2 values of the regression lines were above 0.7 for six of the seven sites (Fig. 3.1). The RMSE increased with increasing COLE values. Only the three clay-textured soils (mean COLE values 0.11, 0.14 and 0.17 m m^{-1}) had visible soil cracks at the end of the study, and the slopes of the regression lines of change in layer thickness with change in water content were similar within cracking sites and within non-cracking sites (Fig. 3.1), with the sandy clay loam site (COLE = 0.08 m m^{-1}) being the exception. The sandy clay loam did not lose as much water as the clay sites, and it is possible that this site would have cracked if it had lost a sufficient amount of water from the soil.

Our measurement method of soil layer thickness (Chapter II) was sensitive enough to detect the slight soil shrinkage in the low-COLE fine sandy loam of around 1 mm for an approximately 20 cm soil layer (Table 3.2), giving us confidence in

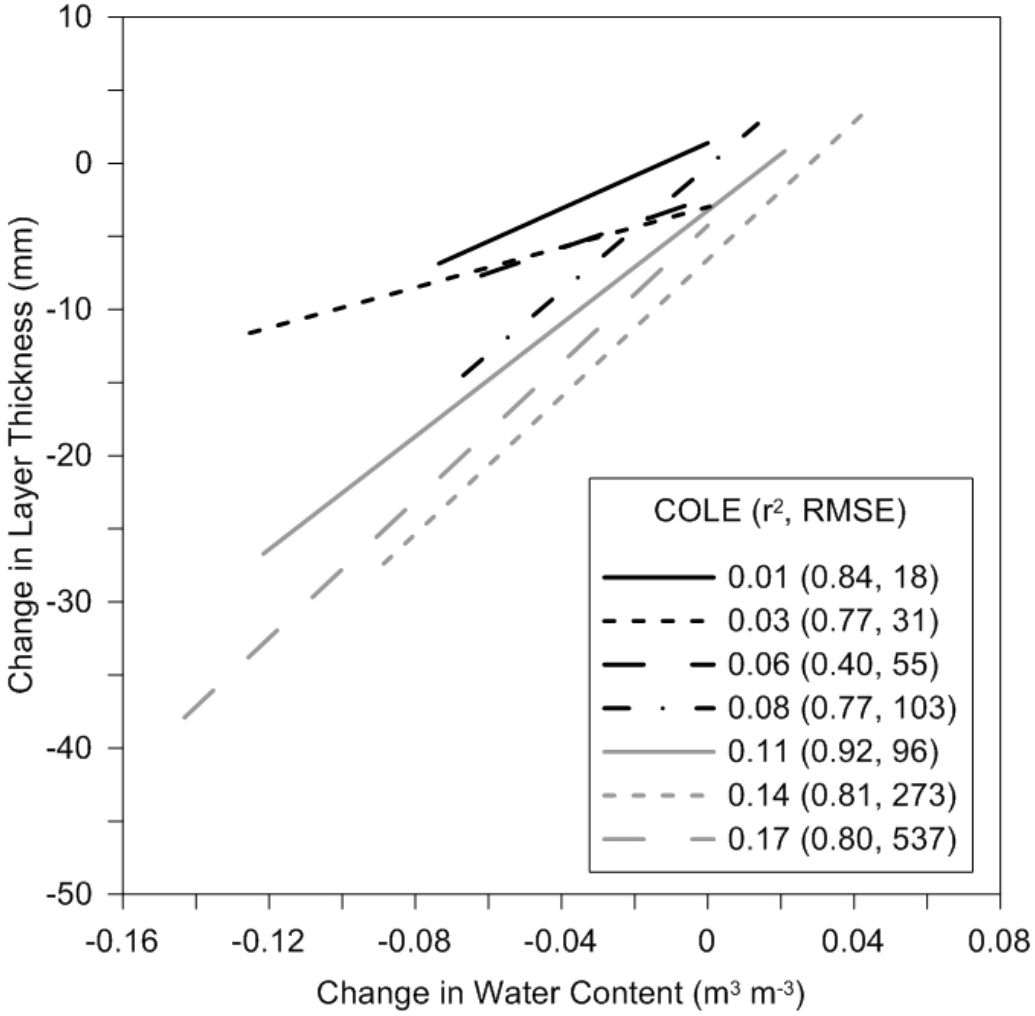

Figure 3.1. The regression lines of measured changes in water content vs. changes in layer thickness of a 1-m deep soil profile for the seven soils. Lines represent each pedon and are bounded by the data range. Sites are labeled by mean pedon COLE (m m^{-1}) value, with r^2 for each regression line and root mean squared error (RMSE, mm). Black lines represent sites that had no visible soil cracks, and grey lines represent sites that were visibly cracked.

this method for measuring *in situ* soil shrinkage. This accuracy was an improvement over measurement systems used by Kirby et al. (2003), who only saw clear trends between water content and vertical shrinkage when the wetting and drying trends were

Table 3.2. Soil water contents and layer thickness means for the four boreholes at each site.

Soil	Depth (mm)	COLE ($m\ m^{-1}$)	θ ($m^3\ m^{-3}$)			Layer Thickness (mm)			Areal Volume of Cracks ($mm^3\ mm^{-2}$)		
			θ_0	θ_{End}	θ_{-1500}	L_0	L_{End}	L_{-1500}	AVC_L	$AVC_{COLE,\theta}$	AVC_{cement}
Fine sandy loam	50	0.01	0.11	0.05	0.05	100.5	94.3	99.5	17.4	3.0	0
	150	0.01	0.11	0.05	0.05	91.3	91.7	90.4	-1.0	2.9	0
	300	0.01	0.12	0.06	0.05	201.0	201.0	199.0	0.0	5.5	0
	500	0.01	0.13	0.06	0.05	200.0	199.3	198.0	2.0	5.1	0
	700	0.01	0.14	0.06	0.05	204.0	203.3	202.0	2.0	5.3	0
	900	0.01	0.16	0.07	0.05	196.8	195.3	194.9	4.5	4.7	0
Silt loam	50	0.04	0.18	0.03	0.07	93.7	88.4	90.1	14.9	13.9	0
	150	0.04	0.22	0.09	0.07	106.1	103.1	102.0	8.7	10.6	0
	300	0.02	0.24	0.11	0.07	192.3	190.3	188.6	5.9	8.5	0
	500	0.02	0.21	0.10	0.07	200.7	199.3	196.7	4.2	9.3	0
	700	0.02	0.21	0.09	0.07	201.9	201.0	198.0	2.7	9.9	0
	900	0.02	0.20	0.09	0.07	199.8	199.9	195.9	-0.3	9.7	0
Silty clay loam	50	0.07	0.21	0.09	0.07	93.6	89.1	87.5	12.9	15.3	0
	150	0.07	0.28	0.18	0.07	95.9	94.4	89.7	4.4	8.6	0
	300	0.02	0.31	0.23	0.07	202.7	200.6	198.7	6.4	3.9	0
	500	0.02	0.33	0.29	0.07	198.9	198.6	195.0	1.0	2.0	0
	700	0.04	0.35	0.32	0.07	201.3	201.1	193.6	0.7	1.8	0
	900	0.04	0.36	0.34	0.07	200.3	197.4	192.6	8.4	1.7	0
Sandy clay loam	50	0.10	0.24	0.20	0.10	95.3	91.7	86.6	10.4	7.0	0
	150	0.10	0.28	0.21	0.10	99.5	93.5	90.5	16.9	10.8	0
	300	0.08	0.33	0.25	0.10	198.5	192.9	183.8	16.3	14.2	0
	500	0.08	0.33	0.25	0.10	198.0	194.8	183.3	9.3	13.9	0
	700	0.06	0.30	0.22	0.06	200.1	198.9	188.8	3.5	12.0	0
	900	0.06	0.26	0.16	0.06	199.2	198.0	187.9	3.5	16.3	0
Clay	50	0.11	0.31	0.14	0.17	88.8	79.3	79.6	25.6	28.7	1.2
	150	0.10	0.36	0.19	0.17	98.5	94.8	89.2	10.8	23.3	1.3
	300	0.10	0.40	0.25	0.17	199.4	195.8	181.2	10.8	33.1	1.2
	500	0.11	0.42	0.30	0.17	200.2	196.0	181.0	12.4	26.5	0.4
	700	0.11	0.42	0.33	0.17	201.7	199.0	182.1	7.9	20.6	0.4
	900	0.11	0.42	0.36	0.17	199.4	196.3	180.5	9.3	12.5	0.2
Clay	50	0.14	0.27	0.27	0.23	77.6	79.7	68.0	-6.6	0.8	0.9
	150	0.14	0.33	0.26	0.23	95.5	87.6	83.5	21.8	21.4	1.7
	300	0.14	0.38	0.30	0.23	193.8	187.9	170.5	17.1	33.8	2.1
	500	0.14	0.40	0.34	0.23	196.7	187.7	172.9	25.8	26.9	1.6
	700	0.15	0.40	0.34	0.23	199.5	187.7	173.6	33.4	26.5	1.1
	900	0.16	0.39	0.34	0.23	196.5	184.2	170.1	34.6	22.3	0.5
Clay	50	0.16	0.45	0.22	0.25	81.4	75.3	69.9	16.8	33.0	3.4
	150	0.16	0.40	0.21	0.25	99.1	92.6	85.1	18.2	44.8	3.6
	300	0.17	0.45	0.30	0.25	200.6	189.4	171.8	31.5	59.0	6.4
	500	0.17	0.49	0.34	0.25	199.3	190.7	170.7	24.9	50.3	5.7
	700	0.17	0.50	0.36	0.25	202.7	195.2	173.6	21.7	45.1	5.0
	900	0.17	0.50	0.38	0.25	200.3	195.6	171.5	13.8	37.8	5.0

strong, and Dinka et al. (2013) where shrinkage of individual soil layers could not be resolved. Some soil cracking was observed around the access tubes, which increased uncertainty in the water contents measured by the neutron moisture meter (Jarvis and

Leeds-Harrison, 1987). Without *a priori* knowledge of the volume of soil cracks around the access tubes, it was impossible to quantify the uncertainty of soil water content measurements. However, volumetric water content at the end of the study was rarely lower than the NCSS database θ_{-1500}, and these exceptions were in the surface layers only. The largest difference in water content between wilting point and the water content at the end of the study was 0.04 m^3 m^{-3}, which is not far from the RMSE of the neutron moisture meter calibration. Overall, there were no unreasonable soil water content values, and no sudden decreases in water content indicating a large crack opening suddenly. Although this model is intended to use available soil data, local measurements of COLE were used for model inputs because at least one site was misidentified by the NRCS soil map (Table 3.1); this was not unusual because soil maps are often not accurate at the meter scale (Soil Survey Staff, 2014).

The increase in RMSE of the regression lines (Fig. 3.1) with increasing COLE values is likely due to increasing spatial variability in the shrink-swell process. The standard deviation among boreholes increased for both layer thickness and water content measurements with increasing COLE values (data not shown). Measurements of shrink-swell and water content over time within a single site showed the standard deviation of soil layer thickness among boreholes increased during wetting events and tended to decrease throughout the dry-downs. In contrast, standard deviation of water content, as measured by the neutron moisture meter, was lowest during wetting events and highest at the end of the study. After irrigation events, an increase in soil water content was observed before the soil would swell, and the time lag was longer for the clay soils

compared to coarser textured soils, about 24 to 48 hours for clay surface layers. While the neutron moisture meter measures bulk soil water content, the soil only swells once water adsorbs to the surface of clay particles in the soil matrix (Wilding and Tessier, 1988). The slower redistribution of water from inter-pedal to the matrix in clay soils compared with coarser textured soils is likely due to decreased hydraulic conductivity of clay soil and clay films. The lag time has been observed by others (Arnold et al., 2005), and is likely a function of soil matrix hydraulic conductivity.

Additional variability in the relationship between soil layer thickness and water content may result from different sample supports, or the volume of the sample, of the two measurement methods (Western and Bloschl, 1999). Although measurements of layer thickness and water content were co-located in the same borehole, the support for water content measurements was a larger volume of soil than for soil layer thickness. Because the distribution of soil water is highly variable in space and time (Cabidoche and Voltz, 1995; Towner, 1968), soil layers are likely not experiencing homogeneous drying or wetting conditions. The water content of different volumes of soil, even overlapping volumes of soil, might be slightly different because of this. This occurs partly due to the preferential flow of water through inter-pedal space coupled with slow infiltration into the soil matrix, causing highly localized shrink-swell processes on the centimeter scale or smaller (Favre et al., 1997). In addition to heterogeneity in soil water content, the shrink-swell process depends on more than water content. Soil swelling may occur rapidly in unconfined areas, such as filling in a crack where soil pressure is zero, but swelling of the bulk soil is expected to be a slower process as water pressure on

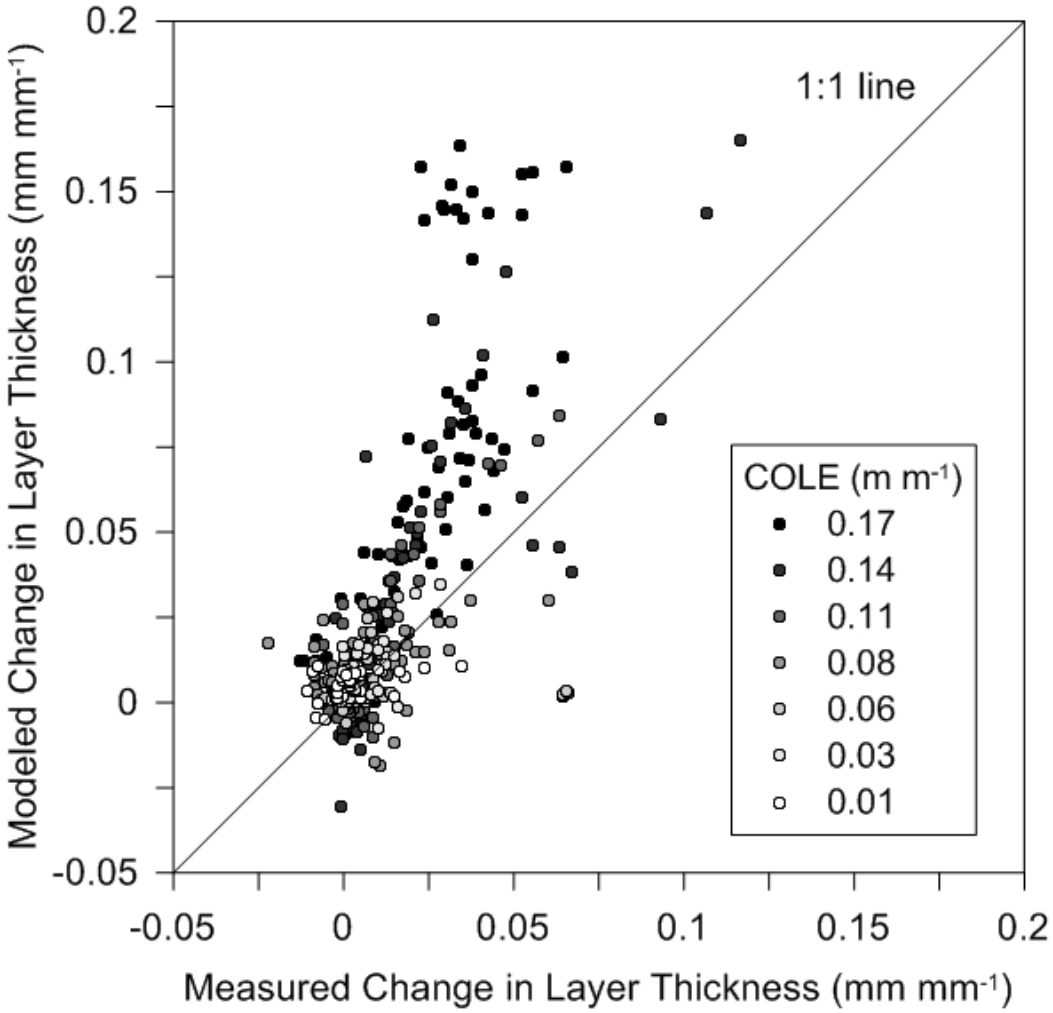

Figure 3.2. Measured change in layer thickness (ΔL) vs. modeled change in layer thickness ($\Delta L_{COLE,\theta}$) for all soil layers and measurement dates. All changes in thickness are relative to the initial layer thickness for that individual soil layer. Sites are labeled by mean pedon COLE values.

soil particles pushes against gravity and overburden pressure. Soil swelling continued for more than 50 days under ponded conditions (McIntyre, 1982), but cracks closed within hours of irrigating in another study (Favre et al., 1997). The high degree of spatial variability and complex shrink-swell process make in situ shrinkage curves

difficult, but it is important to get our measurement efforts out of the laboratory and *in situ*.

The modeled change in layer thickness, based on COLE and water content ($\Delta L_{COLE,\theta}$) tended to overestimate measured values (Fig. 3.2). For comparison, all changes in layer thickness were made relative to initial layer thickness for that individual soil layer. The majority of the overestimates occurred in the most developed and strongest structured horizons (clay, mean COLE = 0.17 m m^{-1}). It is likely that the soil structure help the soil pedon "resist" subsidence.

Estimating the change in soil layer thickness through soil properties has many applications, but this study was focused on its use in estimating soil crack volume. Both the Bronswijk approximation (AVC_L) and the modified Bronswijk approximation ($AVC_{COLE,\theta}$) were compared with the photographically-estimated soil crack volume (AVC_{cement}) (Fig. 3.3). Points with zero measured crack volume were sites that did not have visible surface soil cracks; even though all soils shrank vertically, only three of the seven sites had visible surface cracks. The modified Bronswijk approximation, using COLE and water content, was a better fit to AVC_{cement} than using measurements of change in layer thickness (AVC_L); regression lines were calculated excluding non-cracking sites. The $AVC_{COLE,\theta}$ prediction was a closer fit to AVC_{cement} than soil shrinkage measurements alone (AVC_L) likely because the measurement scale of $AVC_{COLE,\theta}$ was closer to the measurement scale of AVC_{cement} than AVC_L. The support-scale for neutron moisture meter measurements is much larger than the magnets. Also, measurements of water content were a volume loss of water and may be more accurate

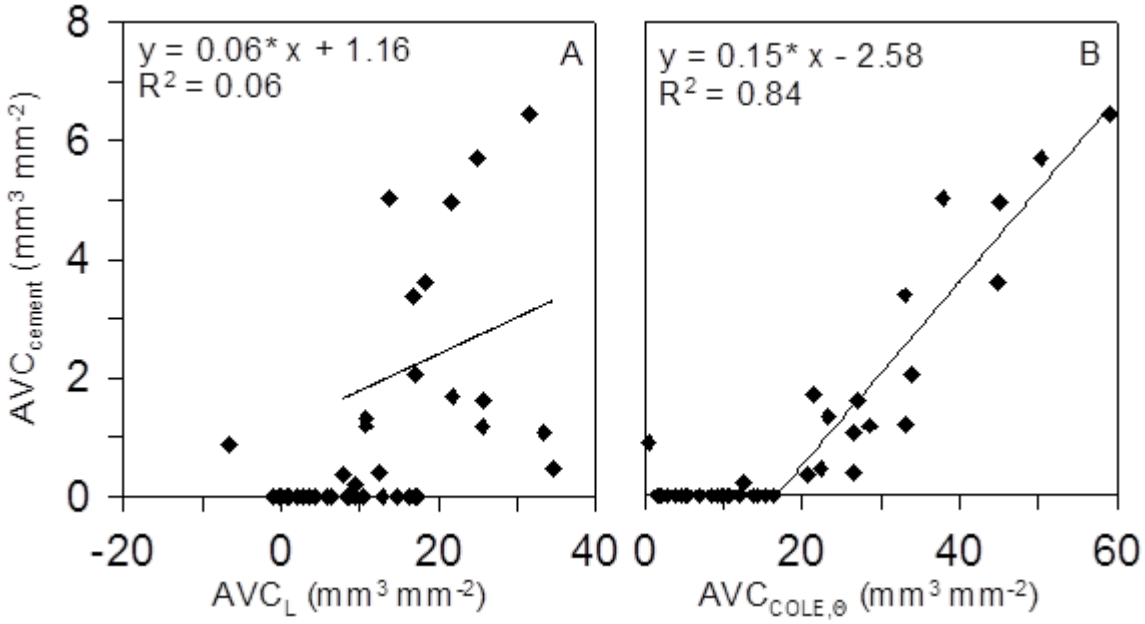

Figure 3.3. Photographically-estimated areal volume of soil cracks (AVC_{cement}) is compared with A) modeled areal volume of cracks from measurements of layer thickness (AVC_L) and B) modeled layer thickness using water content and COLE ($AVC_{COLE,\theta,}$). Points represent the mean of four measurements of each layer for all sites. Regression lines are calculated using only cracking sites.

compared to one-dimensional vertical shrinkage. However, both Bronswijk approximations overestimated AVC_{cement} by a factor of 10. A similar degree of overestimation was found by Rivera (2011) when comparing estimated crack volume from vertical subsidence and measurements of crack depth.

The overestimation of both soil shrinkage and crack volume may be due to either increases in inter-pedal space because of soil structure or anisotropic shrinkage. In a laboratory study, the vertical shrinkage of intact soil cores was less than individual peds (Crescimanno and Provenzano, 1999). As a whole soil shrinks, horizontal cracks, or inter-pedal space, keep layers from 'collapsing.' In soils with strong structure, peds are

distinct from each other and separate from the bulk soil cleanly, which may provide planes of weakness for the soil to crack along. Shrink-swell soils also have slickenside peds, which in addition to their wedge shape, are identified by the directional grooves on their faces, indicating movement along that plane as the soil 'slips.' Because slickensides are tilted between 10 and 60 degrees from horizontal, this slipping is not a completely vertical or horizontal movement, and has been identified as a cause of anisotropic shrinkage in the field (Cabidoche and Voltz, 1995).

The primary cause to the overestimation of AVC_{cement} is likely due to the methodology used. The Bronswijk approximation calculates total porosity based on isotropic shrinkage, but the methodology used to calculate AVC_{cement} measures cracks a few millimeters wide or larger and only crack networks connected to the soil surface. This was useful because these are the cracks that would be capable of capturing runoff during intense rain events. As soil peds shrink, it is likely that inter-pedal space is also increasing in addition to soil crack volume. However, inter-pedal volume is difficult to measure. The fraction inter-pedal space participating in preferential flow may be quite small; Bouma and Dekker (1978) observed only 2% of ped faces in a strongly prismatic soil were stained with dye tracer. Laboratory-measured porosity is also unsatisfactory, because using dye tracers at the core-scale may miss large-scale variability (Beven and Germann, 1982). Although 10% of Bronswijk-approximated porosity was in the large, vertical cracks as measured by the cement method, it is less clear if the remaining porosity is in inter-pedal space or is less than estimated due to anisotropic shrinkage.

In addition to $AVC_{COLE,\theta}$ overestimating AVC_{cement}, Fig. 3.3 provides evidence that a minimum shrinkage volume necessary to generate crack volume exists. The Bronswijk approximation assumes that any soil shrinkage results in soil crack volume; however, it is clear from field observations that not all soils that shrink will have visible surface cracks. In addition, cracking clay soils do not form cracks as soon as they begin drying. Because the potential volume change of a soil is described by the COLE value, I may be able to describe this phenomenon by using a minimum COLE value required for crack formation. Using a soil characterization database from Texas, the mean COLE value for Vertisols is 0.11 m m^{-1} with a standard deviation of 0.04 m m^{-1}. The mean COLE value of soil horizons where slickensides are described is 0.12 m m^{-1} with a standard deviation of 0.03 m m^{-1}. In this study the minimum COLE where cracking occurred was 0.10 m m^{-1}; however, there is a possibility that the sandy clay loam (COLE = 0.08 m m^{-1}) would have cracked if it had lost a sufficient amount of water.

The formation of soil cracks requires both requisite shrinkage potential (COLE) and water loss. These requirements are jointly addressed by the regression-derived intercept of $AVC_{COLE,\theta}$ and AVC_{cement} (Fig. 3.3). According to the $AVC_{COLE,\theta}$-AVC_{cement} regression, after a minimum $AVC_{COLE,\theta}$ of 20 mm^3 mm^{-2} is reached, the soil begins to crack. The resulting crack volume was 10% of $AVC_{COLE,\theta}$. To further test this, $AVC_{COLE,\theta}$ was calculated for the top 20 cm of soil over time. Then, the slope and intercept of the regression were applied to $AVC_{COLE,\theta,}$ giving us $A\widehat{V}C$, which was compared with the visual presence of soil cracks (Fig. 3.4). There was reasonable agreement between $A\widehat{V}C$ and visual crack presence. The intercept was the observable

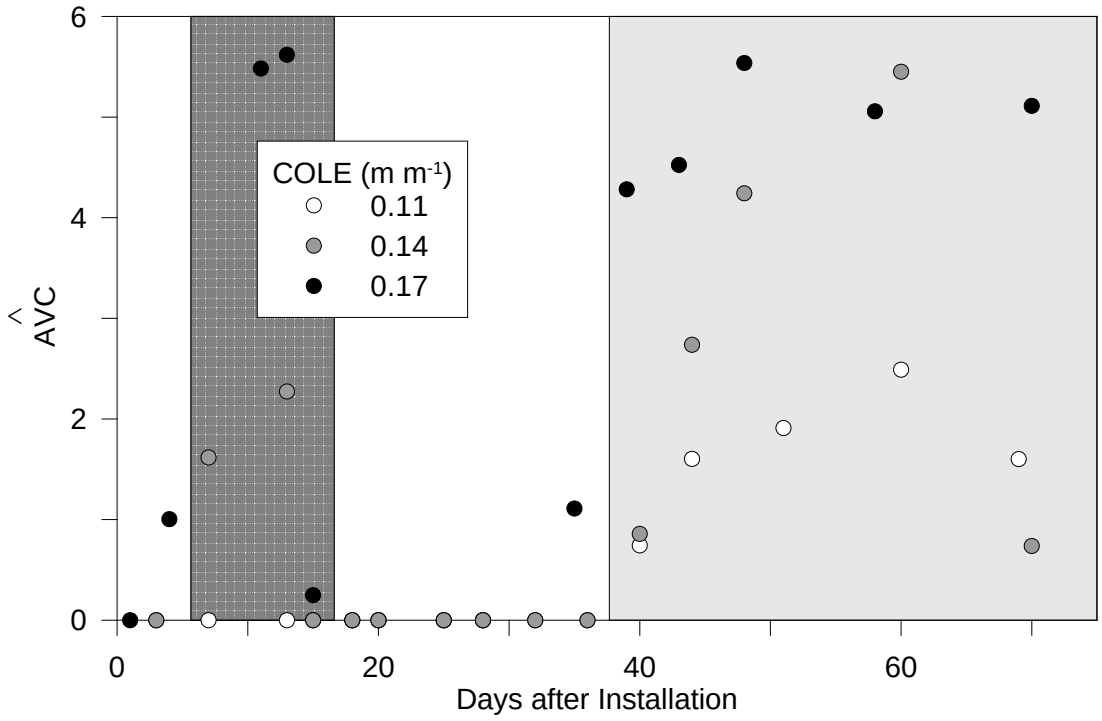

Figure 3.4. Water content measurements for the top 20 cm of soil are used to calculate predicted soil crack volume ($A\widehat{V}C$) for the surface layers over time. Predicted soil crack volume uses the modified Bronswijk approximation ($AVC_{COLE,\theta}$) and the regression line ($A\widehat{V}C = 0.15*AVC_{COLE,\theta} - 2.58$). The cross-hatched area indicates only two sites had surface cracks present (COLE values 0.14 and 0.17 m m^{-1}), and solid shaded areas indicates all three sites had surface cracking present.

lag in time from the beginning of soil water loss to the formation of visible surface cracks. This suggests that there is a minimum shrinkage requirement before soil cracking occurs and the intercept from the regression is describing a mechanistic process of soil shrinkage and crack development. Although more research is needed to fully explain the mechanisms behind *in situ* soil crack behavior, using $A\widehat{V}C$ is a rapid way to predict soil crack volume for soil-water processes and hydrology models.

Conclusions

Although water content and COLE were not reliable predictors of measured soil layer thickness, these soil properties were useful improvements in estimating soil crack volume for seven soils over a range of COLE values from 0 to 0.17 m m^{-1}. COLE can be used to parameterize soil shrinkage models by defining the slope of vertical shrinkage with loss in water content. By using the minimum shrinkage and scaling factor identified by this study, I was able to reasonably predict the presence and absence of surface soil cracks over time. Using soil properties to model soil-water processes is advantageous because it alleviates the need for site-specific calibration, and the NRCS database is an available and reliable source of model parameters.

CHAPTER IV

MAPPING SOIL PROPERTIES ON A VERTISOL USING APPARENT ELECTRICAL CONDUCTIVITY

Introduction

Soils in the Texas Blackland Prairie are a valuable economic and environmental resource because of their agricultural productivity and organic C storage. The Texas Blackland Prairie is an ecoregion of around 50,000 km^2, and includes the large population centers of Dallas and Austin (Griffith et al., 2007). Many of the soils in the Blackland Prairie are Vertisols and Vertic intergrades formed from calcareous marls, chalks, and shales. These soils tend to be high in clay content and shrink and swell with changes in water content, leading to the formation of large cracks capable of capturing runoff during heavy precipitation events. Currently, predicting the amount of runoff and infiltration on these landscapes is difficult due to the spatial variability in soil cracking potential despite the homogeneous clay content generally found on these landscapes (Dinka et al., 2013). Electromagnetic induction, a proximal sensing technique, has been used to map the spatial variability of many soil properties including salinity, clay content and soil water content. However, little is known about what drives the response of electromagnetic induction in Vertisol landscapes. Knowledge of the soil properties that influence electromagnetic induction response on Vertisol landscapes would help assess the usability of these proximal sensors in relatively uniform, high-clay soils. These

sensors would be particularly useful if it responds to the soil properties driving spatial variability in shrink-swell potential.

Soil models are being developed to simulate soil crack formation at the meter-scale across landscapes using information on soil properties, particularly shrink-swell potential, as well as the thickness of the soil solum (Lepore et al, 2009, Chapter III). However, the database of information for these models is often mapped at coarse spatial scales (1:24,000). To take advantage of models that are capable of accounting for fine-scale soil variability (10 m), proximal sensing can be used to refine spatial resolution of soil property information. Shrink-swell potential of the soil is measured in the laboratory and is termed the coefficient of linear extensibility (COLE, m m^{-1}), which is the length change of an intact soil ped between field capacity (-33 kPa) and oven dry (105^{o}C). Shrink-swell potential in Vertisols is influenced by clay content and mineralogy (Gray and Allbrook, 2002), land use (Wilding and Tessier, 1988), and inorganic C content (Dinka et al., 2013). In NRCS soil surveys, soil properties, such as COLE, are assigned to soil mapping units along a landscape. The performance of hydrology models that can incorporate variability in soil properties at sub 100-m scales may be improved with soil information at finer spatial spaces.

Fine-scale soil variability has been mapped using proximal sensors (Lund et al., 1999; Johnston et al., 2001; Corwin and Lesch, 2005), and this technique may be useful in mapping soil properties associated with shrink-swell potential. Electromagnetic induction is a common non-contact, proximal sensing technique that measures the bulk apparent electrical conductivity of the soil (EC_a) by inducing a secondary magnetic field

in the soil (McNeil, 1980). A popular electromagnetic induction instrument is the EM38 (Geonics Limited, Mississauga, Ontario, Canada), because its depth of exploration, around 1.5 m, is consistent with the zone of interest in agriculture and critical zone sciences. When used with GPS, EC_a data can be collected at much higher densities than direct methods such as soil cores (McBratney et al., 2005), but should always be validated using soil data. Bulk apparent electrical conductivity measurements of the soil have been used extensively in mapping zones of soil variability for precision agriculture in the Midwestern U.S. (Lund et al., 1999; Johnson et al., 2001; Corwin and Lesch, 2005), and for mapping specific soil properties including salinity, clay content, soil water content (Rhoades et al., 1976; McBride et al., 1990; Corwin and Lesch, 2005; Brevik et al., 2006). However, in the Vertisol landscape of the Texas Blackland Prairie, variability in the response of the EM38 often cannot be explained by these properties.

It is important to note that EC_a is a cumulative response to many soil properties simultaneously, with some properties affecting the measurement more than others. If a more dominant soil property is present, then a less dominant property cannot be mapped accurately (McBratney et al., 2005). The most dominant soil property affecting EC_a in agricultural soils is salinity (Rhoades et al., 1976), but when salinity is low the influence of other soil properties emerges. Complicating the use of the EM38 to map soil properties is the co-correlation of many soil properties, including the relationship between clay content and soil water content. Clay soils have a higher soil water holding capacity than coarser textured soils, and the order of dominance between clay content and soil water content on the EC_a response seems to be site specific.

The majority of the research on the response of the EM38 to soil properties has been done on moderately-fine to coarse-textured agricultural soils. Harvey and Morgan (2009) used the EM38 to predict clay content in Alfisols and Mollisols when clay content varied from 10 to 35%. On fluvial soils ranging from clay textures to gravel, the EM38 could be used to predict clay content under moist soil conditions (Weller et al., 2007); clay content predictions were also possible on landscapes containing clay loams and sandy clay loams, as observed by Carroll and Oliver (2005). However, when clay content was relatively homogeneous, EC_a followed the spatial pattern of topography and soil depth, when soil depths were between 0.2 and 1 m (Serrano et al., 2010). Electromagnetic induction has also been useful in mapping soil water content. In a moderately fine-textured soil in undulating topography, EC_a was strongly correlated with soil water storage (Kachanoski et al., 1990), which may indicate that strongly varying topography drives EC_a response by both soil water distribution and preferential weathering patterns. Bulk apparent electrical conductivity has also been used to map depth to the clay pan in Alfisols, when the clay plan was between 7 and 105 cm from the soil surface (Doolittle et al., 1994), and a response to inorganic C was observed by Kuhn et al. (2009) on a calcareous-sandy landscape. The soil water status may account for some of the differences in these study results, and has been shown to alter the spatial pattern of EC_a (Weller et al., 2007; Harvey and Morgan, 2009; Zhu et al., 2010a; Zhu et al., 2010b). In calcareous Vertisols, I expect the homogeneous clay content across the landscape may lead to other properties becoming important in electromagnetic induction soil mapping. In a Texas Vertisol, Akbar et al. (2004) observed a decrease in EC_a with

decreasing soil solum depth, which was measured as the depth to calcareous parent material. Although the correlation was not strong, it may be the EM38 was actually responding to inorganic C content, as seen by Kuhn et al. (2009).

If the EM38 is responding to changes in inorganic C on Vertisol landscapes, researchers might be able to map shrink-swell potential because inorganic C content is a soil property that is closely related to shrink-swell potential in these soils (Dinka et al., 2013). In the Blackland Prairie, inorganic C concentrations in the soil are largely driven by the extent of weathering of the parent material and translocation of inorganic C, and this differential in inorganic C location relative to the soil surface can occur on the 10-m scale. In addition, inorganic C can also vary due to gilgai formation and the associated subsurface chimney and bowl features (Miller et al., 2010), which can vary on the 1-m scale. Gilgai are surface features consisting of small depressions (microlows) separated by ridges (microhighs), and often coincide with surface topography and include increased clay content and organic C in the bowls/microlows and increased inorganic C in the chimneys/microhighs. The scale of these features is usually between 3 and 10 m. Both landscape variability and gilgai microtopography are finer than NRCS soil survey maps. By identifying the spatial variability of inorganic C on these landscapes, we may be able to begin to quantify the spatial variability of soil shrink-swell potential.

Prior research on how electromagnetic induction may respond to bulk soils properties suggests that electromagnetic induction may be able to map inorganic C. Electrical current can take three paths through the soil: solid phase, liquid phase, and the

liquid/solid interface (Rhoades et al., 1976). Air-filled pore space does not conduct electricity. In its simplest form, EC_a can be separated into two conductors:

$$EC_a = EC_b + EC_s \quad [4.1]$$

where EC_b is the conductivity of the liquid phase and EC_s is the surface conductivity of soil particles, or the solid phase (Rhoades et al., 1976). Solid phase conductivity generally increases with increasing clay content and increasing specific surface area of the clay particles and is independent of soil water content. Conversely, quartz sand has little surface conductivity, and its EC_a is directly proportional to the conductivity of the soil solution (Archie, 1942). Inorganic C will likely decrease solid phase conductivity, and therefore decrease overall EC_a independently of water content. In the calcareous Vertisols of the Texas Blackland Prairie, response of EC_a should be driven by changes in inorganic C content.

Overall objectives of this study were to determine the soil properties that contribute to measurements of EC_a in a calcareous Vertisol, and to determine if any of those properties could be used to map variability in the shrink-swell potential of calcareous Vertisols. Many studies have attempted to link EC_a with soil properties using correlation and empirical models. I would argue that models should be based on measurable soil properties with minimal fitting parameters, as in McBratney et al. (2005). The specific objectives of this study were to describe the response of EC_a to soil properties on calcareous Vertisols, and build a quasi-mechanistic model predicting

inorganic C across non-saline Vertic landscapes using proximally-sensed EC_a. The resulting predictions may be useful as a proxy for shrink-swell potential for the improvement of hydrology models on the Texas Blackland Prairie.

Methods and materials

A detailed, small-field study, and a large field study were conducted to evaluate the response of the EM38 to soil properties. The detailed field study looked at multiple soil properties to determine the effect of soil moisture, depth of the solum, and inorganic C on proximally sensed EC_a across a 0.2 ha area with gilgai. The large field study was conducted in two watersheds of 10 and 14 ha each. The large field study only sampled for inorganic C. All study sites were located on the USDA-ARS Grassland, Soil and Water Research Laboratory watershed network near Riesel, TX (Fig. 4.1).

Detailed field study

A small, 40- by 50-m area of a Houston Black clay (fine, smectitic, thermic Udic Haplusterts), had not been plowed for over 30 years and had circular gilgai microtopography. The electromagnetic induction survey and soil sampling was conducted on 11 March 2011, when the field was close to field capacity, and on 11 Sept. 2011, under dry soil conditions. An EM38 sensor in the vertical dipole mode only, was used to measure EC_a in combination with an AgGPS for geo-referencing (Trimble Navigation Limited, Sunnyvale, CA). In the vertical dipole mode, the EM38 senses from 1.5 to 2 m deep, with a sampling area of approximately 1 m^2 (McNeil, 1980). Both surveys were walked on 1-m, parallel transects while logging EC_a measurements automatically every second. Instrument drift was assessed by having one location

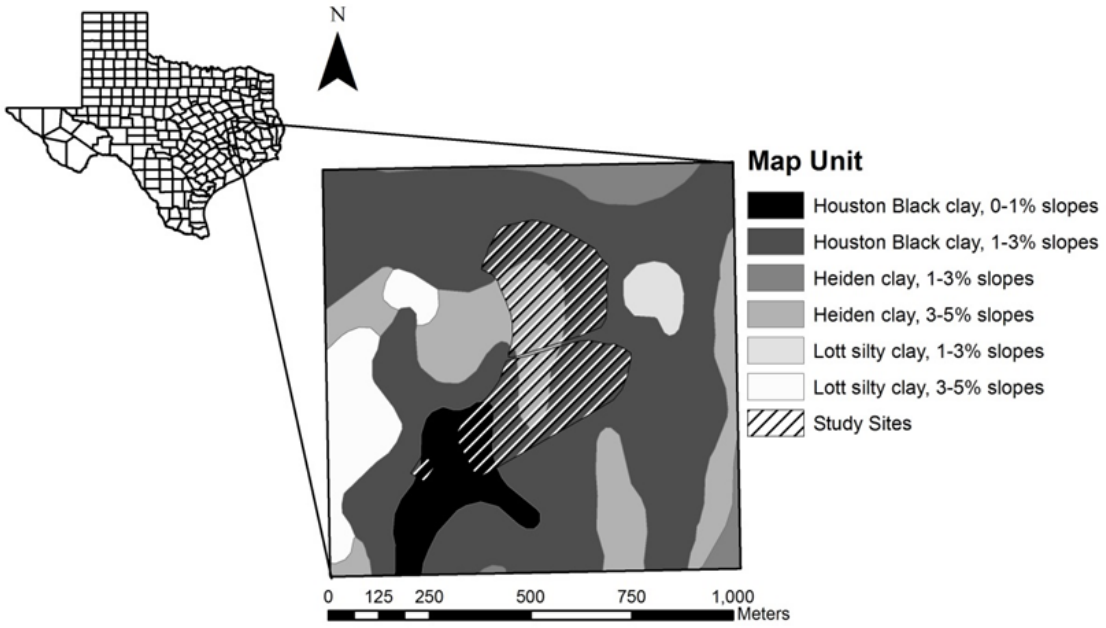

Figure 4.1. Study site located near Riesel, Texas, on the USDA-ARS Grassland, Soil and Water Research Laboratory.

marked for measurements before and after surveys, and soil temperature was recorded 5 cm below the soil surface before and after surveys. All surveys were standardized to 25°C using the Sheets and Hendricx (1995) correction,

$$EC_{25} = EC_T * \left(0.4470 + 1.4034e^{-T/26.815}\right), \quad [4.2]$$

where EC_T is the EC_a data collected, and T is the measured soil temperature (°C).

Geo-referenced soil samples were collected for soil water content at the time of each survey, plus soil properties including clay content, soil depth, inorganic C content, and electrical conductivity of the soil solution were measured in the laboratory. Sampling locations across the field were chosen to capture the range of EC_a measurements and gilgai positions. At each sampling location, two cores were taken within 0.5 m distance. One core was taken for soil water content and cut at 10-cm intervals, and the other was cut into 20-cm sections and air-dried for soil property analysis. Soil cores were taken to a depth of 2 m or to the weathered marl. Soil core sections were ground and passed through a 2-mm sieve. Soil analysis methods included inorganic C content (Sherrod et al., 2002), electrical conductivity of the soil solution, and soil particle size. Electrical conductivity of the soil solution was performed using a multicell conductivity probe (545, Amber Science Inc., Eugene, OR) with 1:2 soil to water extract (Rhoades, 1982). Soil particle size distribution was measured using the pipette method (Kilmer and Alexander, 1949). A total of 16 sampling sites were selected for the March survey. During the September survey, 8 of the 16 original sampling locations were selected and soil cores for soil water content were collected.

Large field study

To test EC_a response at a larger spatial scale, two additional surveys using the EM38 in the vertical dipole model were conducted at approximately field capacity. Surveys were conducted in January 2007 (Field 1) and March 2006 (Field 2) using 10-m transect spacing. Soils consisted of a Houston Black clay (fine, smectitic, thermic Udic Haplusterts) and a Heiden clay (fine, smectitic, thermic Udic Haplusterts). The EM38

was pulled on a sled with an all-terrain vehicle, and both surveys were temperature corrected using Eq. [4.2] (Sheets and Hendricx, 1995). Field 1 was a 14 ha field that has been terraced and cropped annually in a corn and wheat rotation. Immediately to the north is Field 2, a 10-ha field which was in perennial, grazed pastureland. Thirty-nine soil cores were collected and analyzed for inorganic C, 24 from Field 1, and 15 from Field 2.

Results and discussion

Detailed field study

The spatial pattern of proximally-sensed EC_a visually correlated with gilgai position and shape across the study site for the March (moist conditions) survey, and the visual assessment of gilgai presence in the September EC_a was less defined (Fig. 4.2). Bulk apparent electrical conductivity was higher and greater in range in March (65 to 145 mS m^{-1}) when the soil was moist compared with September (7 to 32 mS m^{-1}) when the soil was dry.

The contribution of soil properties to the response of the EM38 was not equal with depth, and the depth of maximum contribution appeared to change with water content, soil texture, and other properties (McNeil, 1980). The relative influence of soil properties at depth on EC_a can be modeled by the theoretical response curve,

$$EC_a = \frac{4z}{(4z^2 + 1)^{3/2}}, \qquad [4.3]$$

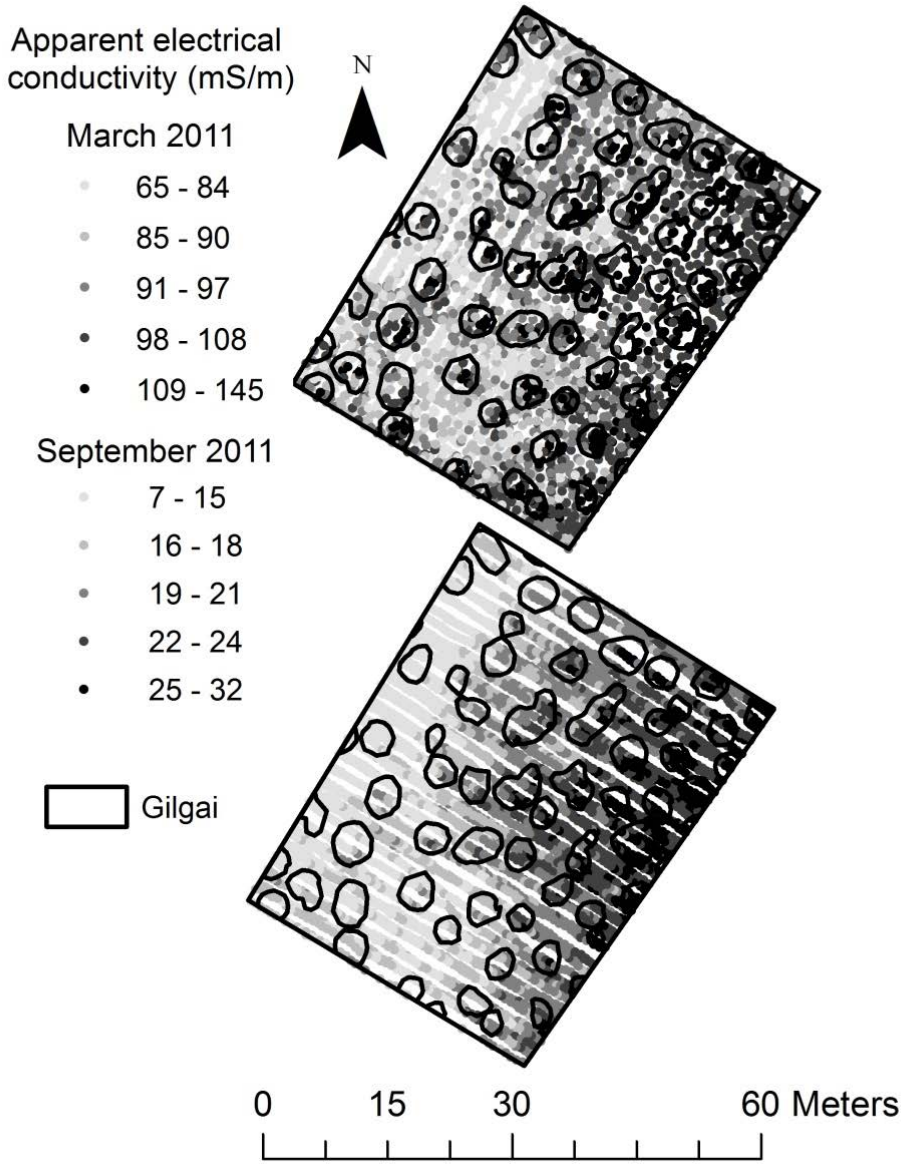

Figure 4.2. Apparent electrical conductivity and sampling locations for the detailed field study. Apparent electrical conductivity is from moist (March) and dry (September) surveys.

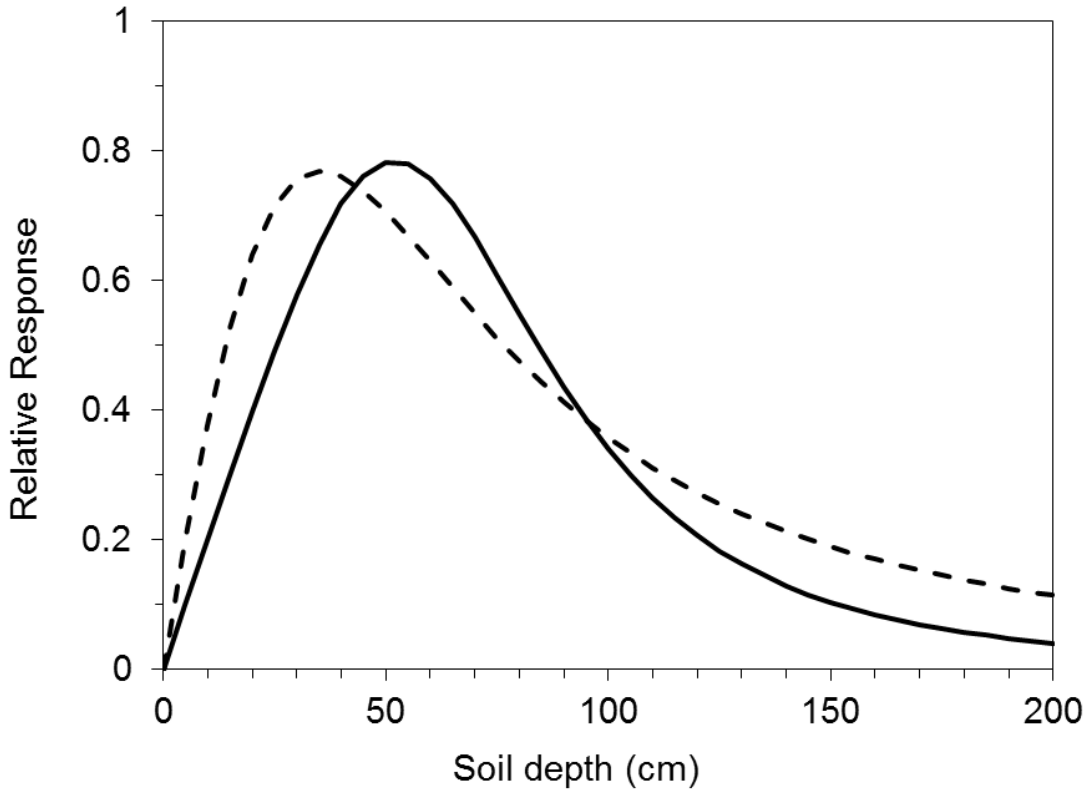

Figure 4.3. Relative response of the EM38 with soil depth (cm). Dashed line is the theoretical response curve published by McNeil (1980), and the solid line is our proposed modification based on soil data.

where z is depth (m) from the soil surface (McNeil, 1980; Fig. 4.3). This function predicts maximum sensitivity at 35 cm from the soil surface. In developing simple correlations between EC_a measurements and soil properties, depth weighting soil properties to match an assumed response with depth of the instrument usually improves correlations (Harvey and Morgan, 2009). Attempting to correlate a given soil property at a depth where the EC_a measurements was not made can lead to the wrong conclusions.

Table 4.1. Pearson's correlation coefficient between soil water content, measured at 10-cm depth increments and bulk apparent electrical conductivity measured using the EM38. Significance is reported at the 0.1, 0.05, and 0.001 p-value for correlation coefficients with *, **, and ***, respectively.

	March (moist)	September (dry)	March (moist)	
Depth (cm)	All	All	Highs	Lows
10	0.61**	0.35	-0.04	0.28
20	0.69**	0.04	0.18	0.05
30	0.70**	-0.16	0.50	0.25
40	0.65**	-0.26	0.36	0.03
50	0.52*	0.11	0.44	-0.01
60	0.84***	0.00	0.93**	0.30
70	0.51*	0.35	0.27	-0.12
80	0.63**	0.55	0.33	0.46
90	0.13	0.35	0.53	-0.33
100	0.36	-0.18	0.79*	0.03
110	0.17	0.12	0.89**	-0.38
120	0.00	0.62*	0.91**	0.24
130	-0.26	0.26	0.94**	-0.55
140	0.33	-0.39	0.95**	-0.58
150	-0.01	0.20	0.94**	-0.70
160	0.46*	-0.27	0.90**	-0.82
170	0.38	-0.14	0.96**	-0.62
180	-0.29	0.20	--	-0.68
190	-0.78	0.12	--	-0.78
200	-0.38	-0.33	--	-0.38
	n = 16	n = 8	n = 7	n = 9
	n = 16	n = 8	n = 7	n = 9

To determine the depth of maximum sensitivity, Pearson's correlation coefficients were calculated for soil water content (Table 4.1) and inorganic C content (Table 4.2) with depth, for both March and September surveys and by gilgai position. When comparing the March and September surveys, much stronger correlations were

Table 4.2. Pearson's correlation coefficients between inorganic soil C content, measured at 20-cm depth increments, and bulk apparent electrical conductivity measured using the EM38. Significance is reported at the 0.1, 0.05, and 0.001 p-value for correlation coefficients with *, **, and ***, respectively.

	March (moist)	September (dry)	March (moist)	
Depth (cm)	All	All	Highs	Lows
10	0.61**	0.35	-0.04	0.28
20	0.69**	0.04	0.18	0.05
30	0.70**	-0.16	0.50	0.25
40	0.65**	-0.26	0.36	0.03
50	0.52*	0.11	0.44	-0.01
60	0.84***	0.00	0.93**	0.30
70	0.51*	0.35	0.27	-0.12
80	0.63**	0.55	0.33	0.46
90	0.13	0.35	0.53	-0.33
100	0.36	-0.18	0.79*	0.03
110	0.17	0.12	0.89**	-0.38
120	0.00	0.62*	0.91**	0.24
130	-0.26	0.26	0.94**	-0.55
140	0.33	-0.39	0.95**	-0.58
150	-0.01	0.20	0.94**	-0.70
160	0.46*	-0.27	0.90**	-0.82
170	0.38	-0.14	0.96**	-0.62
180	-0.29	0.20	--	-0.68
190	-0.78	0.12	--	-0.78
200	-0.38	-0.33	--	-0.38
	n = 16	n = 8	n = 7	n = 9

microlows. Additionally, the depth of strongest correlation was 60 cm for microhighs (significant) and 80 cm for microlows (not significant). Inorganic C at 120 and 160 cm had the strongest correlation coefficients in March and September, respectively. In contrast with water content, more significant correlation coefficients between EC_a and inorganic C were found in microlows compared to microhighs for both surveys. It

seems the response of the EM38 to water content is driven by the presence of microhighs, but the response to inorganic C occurs in the microlows. Generally in calcareous Vertisols with intact gilgai, the highest water contents are found in the microlows, and the highest inorganic C contents are found in the microhighs (Wilding et al., 1989). It is possible that the EM38 cannot differentiate among the high inorganic C contents of microhighs and high water contents of microlows.

Based on our results, maximum sensitivity of the EM38 in the vertical dipole mode was likely between 30 and 60 cm below the soil surface, with information of inorganic C found at around 100 cm. These results led us to shift the maximum of the response curve down in the soil, and decrease the contribution of deeper horizons by adjusting the constants in the McNeil (1980) function (Eq. [4.3], Fig. 4.3). Profile-averages for soil properties were then calculated using weights based on the new response curve,

$$EC_a = \frac{4z}{(4z^2 + 1)^{1.1}} / 2. \qquad [4.4]$$

Although this shift in the curve did not make a large difference in profile averages due to the soil being fairly homogeneous, in a layered soil this could make a critical difference.

Profile-averages of soil water content ranged from 0.31 to 0.42 $m^3\ m^{-3}$ in March and 0.16 to 0.20 $m^3\ m^{-3}$ in September, and patterns of water content were largely tied to gilgai position with higher water contents found in depressions, and lower water contents on the microhighs. Inorganic C content for the study site ranged from 12 to 45 $g\ kg^{-1}$.

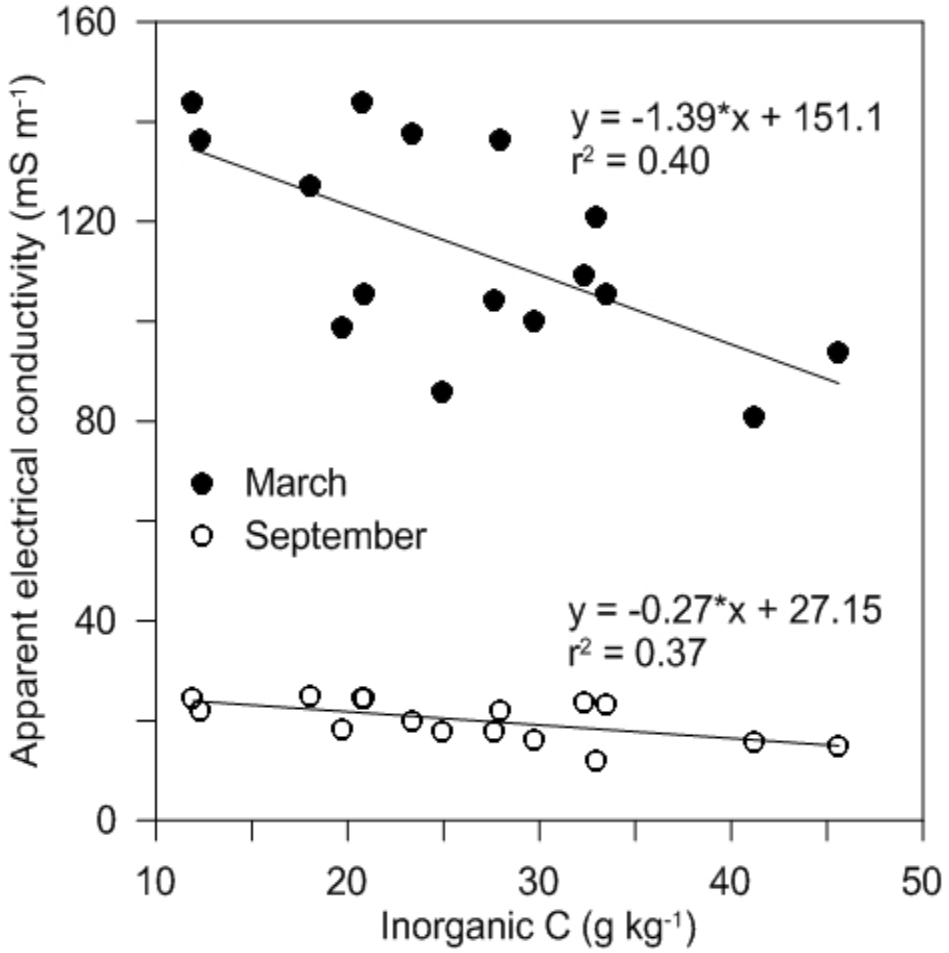

Figure 4.4. Inorganic C vs. apparent electrical conductivity measured in March (moist conditions) and September (dry conditions). Inorganic C contents are depth-weighted profile averages. Both slopes are statistically significant ($p < 0.05$).

The response of EC_a to changes in inorganic C are plotted for both March (moist) and September (dry) surveys. Even though both slopes were statically significant (p-value < 0.05), the March survey had a steeper slope (Fig. 4.4). Higher inorganic C contents were found in microhighs, and lower contents in depressions, which has also been observed

Table 4.3. Pearson's correlation coefficients between bulk apparent electrical conductivity (EC_a), profile averages of soil inorganic C content (IOC) and soil water content, and the depth of the soil solum for March (n = 16) and September (n = 8). Significance is reported at the 0.1, 0.05, and 0.001 p-value for correlation coefficients with *, **, and ***, respectively.

		EC_a (mS m^{-1})	IOC (g kg^{-1})	Water content (m^3 m^{-3})	Soil depth (cm)
March (moist)	EC_a (mS m^{-1})	1			
	IOC (g kg^{-1})	-0.63**	1		
	Water content (m^3 m^{-3})	0.49*	-0.24	1	
	Soil depth (cm)	0.11	0.01	0.56*	1
September (dry)	EC_a (mS m^{-1})	1			
	IOC (g kg^{-1})	-0.60*	1		
	Water content (m^3 m^{-3})	0.13	-0.21	1	
	Soil depth (cm)	0.23	0.00	0.52	1

by Wilding et al. (1989). Electrical conductivity of the soil solution was low and was not significantly correlated with EC_a. Clay content was high, between 45 and 56%, and was not correlated with EC_a for either survey. The depth to parent material was between 80 and 130 cm, with a clear boundary between the solum and weathered calcareous parent material. The spatial patterns of soil properties were consistent with previous findings (Wilding et al., 1989; Coulombe et al., 1996) and corresponded to position in the microtopography.

To investigate the relationship between EC_a and soil properties, correlations among profile-averages of water content and inorganic C content, depth to weathered parent material (or depth of solum) and measurements of EC_a were made for both

Table 4.4. Pearson's partial correlation coefficients while controlling for inorganic C for March (n = 16) and September (n = 8). Significance is reported at the 0.1, 0.05, and 0.001 p-value for correlation coefficients with *, **, and ***, respectively.

		EC_a (mS m^{-1})	Water content (m^3 m^{-3})	Soil depth (cm)
March (moist)	EC_a (mS m^{-1})	1		
	Water content (m^3 m^{-3})	0.45	1	
	Soil depth (cm)	0.15	0.58*	1
September (dry)	EC_a (mS m^{-1})	1		
	Water content (m^3 m^{-3})	<0.00	1	
	Soil depth (cm)	0.40	0.58	1

surveys (Table 4.3). In March (moist conditions), both soil water content and inorganic C were significantly correlated with EC_a, but in September, only inorganic C was significantly correlated with EC_a. Depth to parent material was not well correlated to EC_a, likely because the soil solum was 80 to 200 cm thick, deeper than the EM38's most sensitive depths; however, the correlation was slightly stronger in September. In previous research that correlated soil depth with EC_a, soil depths ranged from 40 to 120 cm (Akbar et al., 2004), which was in range of the EM38. Water content was negatively correlated with inorganic C, suggesting that the inorganic C effect on EC_a may be from both bulk properties of inorganic C in the soil and soil water holding capacity.

If higher concentrations of inorganic C were found in landscape positions that typically had lower water contents, then the response of the EM38 would not only be

due to the increases in inorganic C, but also the decreases in water content. This co-correlation phenomenon is common in EC_a measurements of clay content and water content, where the independent effects of increasing clay vs. increasing water contents are difficult to separate under field conditions (Weller et al., 2007; Harvey and Morgan, 2009). Although the correlation coefficient between EC_a and water content was significant (Table 4.3, $p < 0.10$), the partial correlation coefficient, when controlling for inorganic C, was slightly lower and was not statistically significant (Table 4.4). However, the strong correlation of inorganic C with EC_a in September (dry survey), absent of strong EC_a-water content correlation, suggests that inorganic C has an independent effect on EC_a measurements. Because inorganic C decreases shrink-swell potential, inorganic C could be used as a proxy for mapping shrink-swell potential across non-saline Vertisol landscapes.

Large field study

The same profile-averages were calculated for inorganic C as the detailed, smaller area study, and point EC_a data was interpolated using a tension spline on a 0.25-m grid in ArcGIS v.10.0 (ESRI, Redlands, CA, Fig. 4.5). The terraces of Field 1 were visible on the EC_a maps as linear features, although some landscape trends in EC_a are still intact. For example, higher EC_a values are seen along the concave portion of the footslope. In Field 2, lower EC_a values were found on the shoulders with the highest values found on footslope. Inorganic C was negatively correlated with EC_a in both fields; however, the linear relationship is better defined in Field 2 (Fig. 4.6). Although two separate regression equations were calculated based on least squares regression,

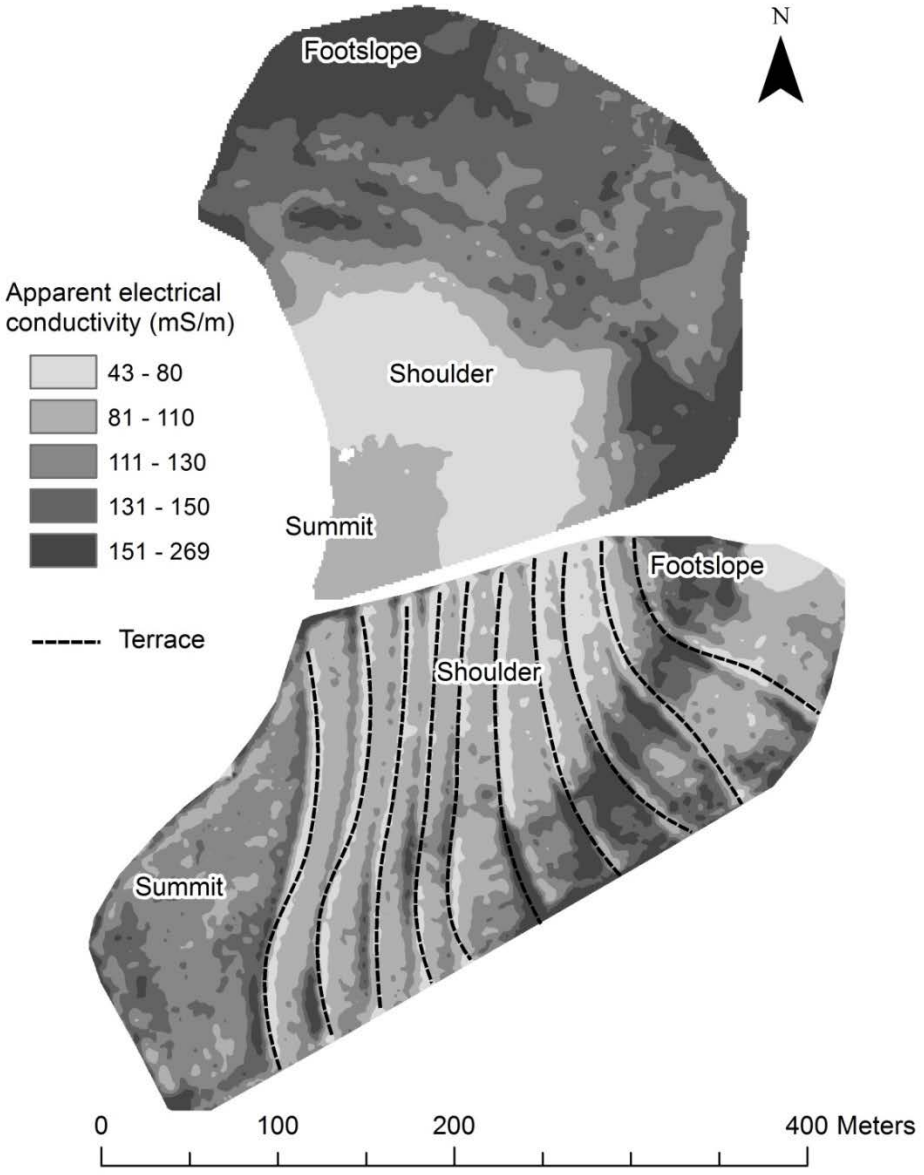

Figure 4.5. Bulk apparent electrical conductivity for the large field study, Field 1 (South) and Field 2 (North).

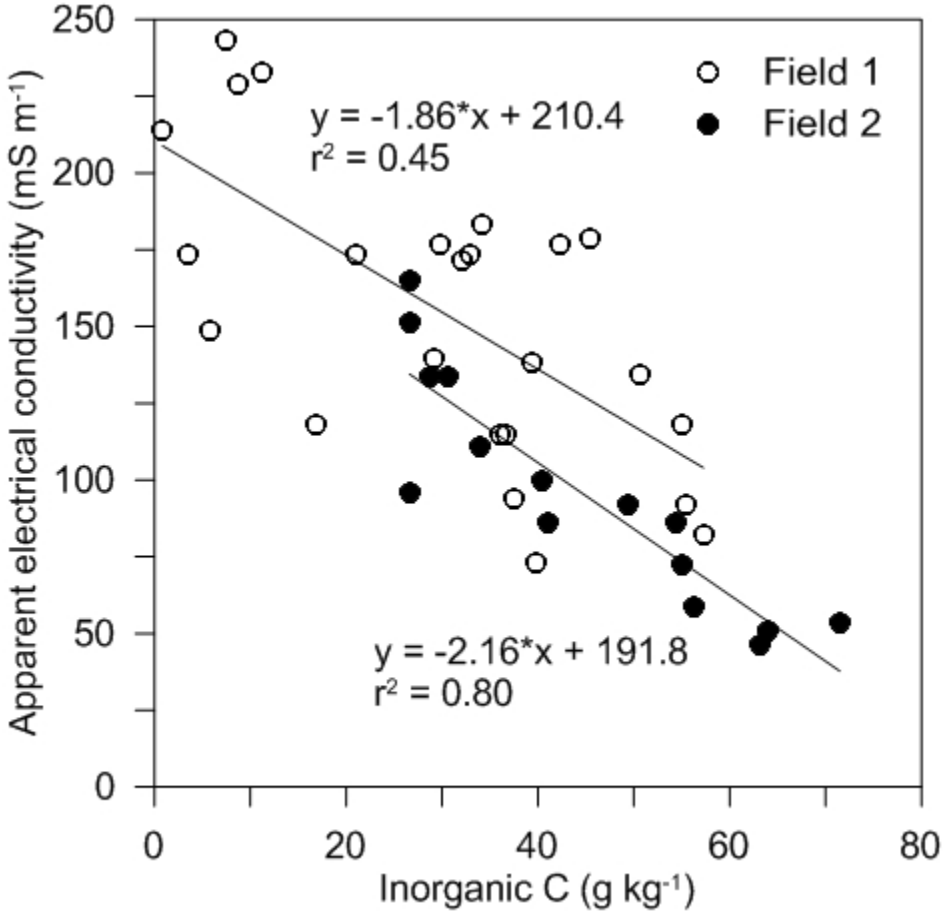

Figure 4.6. Inorganic C vs. bulk apparent electrical conductivity for Fields 1 and 2. Inorganic C contents are profile-averages. Slopes are statistically significant (p-value < 0.001).

neither the slopes (p-value = 0.51) nor intercepts (p-value = 0.65) were statistically different from each other.

Terracing Field 1 has redistributed soil water differently than it would have on the same un-terraced landscape. Although the fields were adjacent to each other and contained soils in the same mapping units, the manipulation of the landscape introduced more short-interval variability, potentially complicating our ability to establish a clear response of EC_a to soil properties.

Predicting inorganic C

In the model from McBratney et al. (2005), which is limited to non-saline soils, EC_a measurements were established to be a function of clay content (%), soil water content normalized by the saturated water content (θ_s) and cation exchange capacity (CEC) normalized to the cation exchange capacity of the reference soil (CEC_0). A fitting factor (κ, units of mS m^{-1}) is used to calibrate the model,

$$EC_a = \kappa * \frac{Clay}{100} * \frac{\theta}{\theta_s} * \frac{CEC}{CEC_0}. \quad [4.5]$$

The model was then used to predict clay content from EC_a data, using surveys under field capacity conditions, and pedotransfer functions to calculate CEC. Because clay content was the most variable soil property in their case, McBratney et al. (2005) argued that EC_a could be used as the prediction variable.

Because in the context of electromagnetic induction surveys on non-saline Vertisols inorganic C is the most variable soil property that has a significant effect on EC_a measurements in calcareous Vertisols, the equation may be modified and use it to model inorganic C. Instead of using pedotransfer functions, I used data from the NRCS database for clay content, and saturated water content. Then, EC_a for each location ($EC_{a,i,j}$) is then relative to EC_{a0} of the field, where EC_{a0} is the scaling factor that represents EC_a of this soil with no inorganic C. The resulting equation,

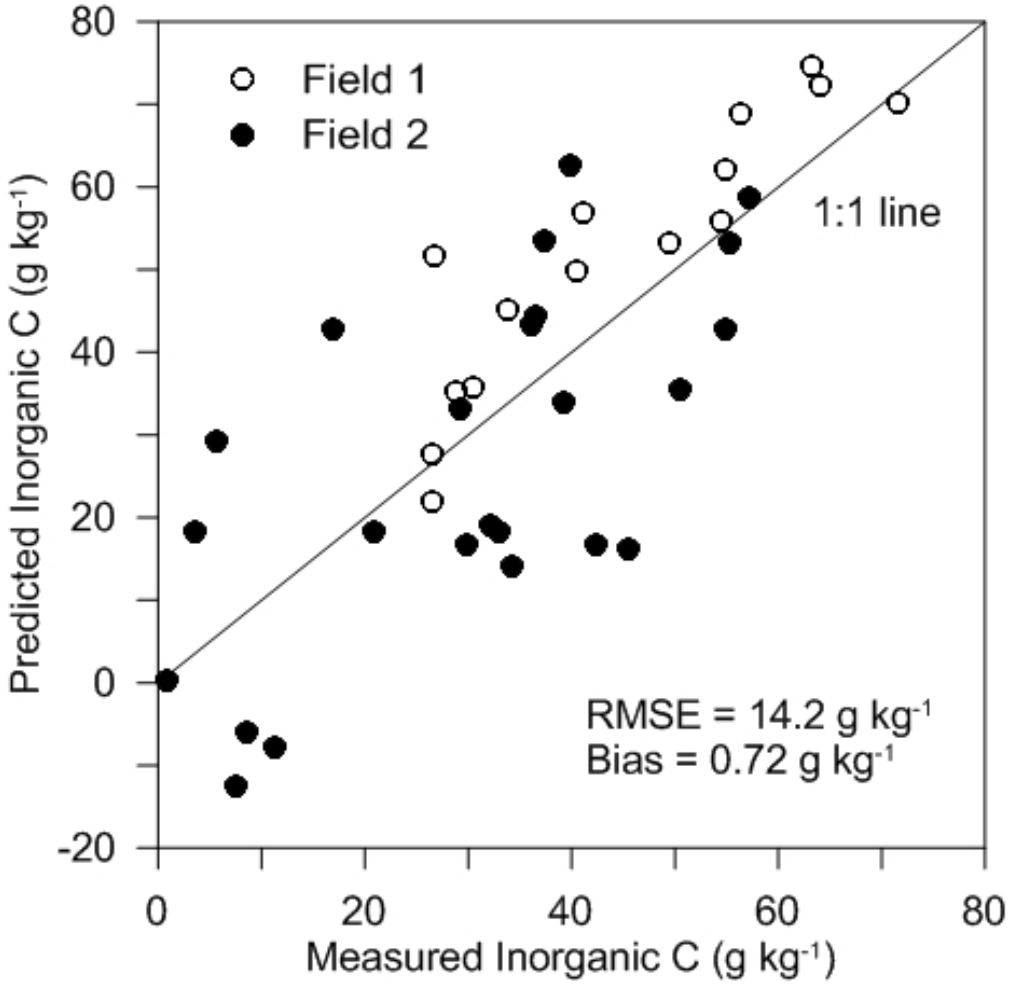

Figure 4.7. Measured vs. predicted inorganic C for Fields 1 and 2.

$$\widehat{\mathrm{IOC}}_{\mathrm{i,j}} = \kappa * \frac{\left(\mathrm{EC_{a0}} - \mathrm{EC}_{a,i,j}\right)}{\mathrm{EC_{a0}}} * \frac{\mathrm{Clay}}{100} * \frac{\theta}{\theta_s}, \qquad [4.6]$$

predicts inorganic C as a function of EC_a, where EC_{a0} is the intercept of the regression of EC_a and measured inorganic C and $EC_{a,i,j}$ is the measured EC_a for each location. The

fitting factor (κ, units mS m^{-1}) was used to fit the data to the model as in McBratney et al. (2005) by minimizing the model's root mean squared error (RMSE).

We used the model for the large field study, using NRCS data from soil mapping units and measurements of EC_a. Clay content was 55 and 50 (%) for Houston Black and Heiden units respectively. Soil water content was assumed to be 0.30 m^3 m^{-3}, and the saturated water content, θ_s, was reported at 0.40 m^3 m^{-3} for Houston Black map units and 0.37 m^3 m^{-3} for Heiden map units. The model of predicted inorganic C using Eq. [6] were compared with measured values (Fig. 4.7); the model had an RMSE of 14.2 g kg^{-1} and tended to over-predict inorganic C from EC_a data. In this model, clay content only varied by soil mapping unit; it is likely that improvements could be seen with a finer-scale map of clay content. Other proximal sensing instrumentation, such as gamma-ray spectrometry, has been shown to respond to clay content (van der Klooster et al., 2011) and may help improve this simple model.

Conclusions

In this study, measurements of EC_a in calcareous Vertisols were correlated with inorganic C and water content, but not clay content or depth to parent material. In soils developed from calcareous parent materials, such as in the Texas Blackland Prairie, EC_a can be used to detect changes in inorganic C at the 1-m and 10-m scale as long as clay content is relatively uniform (between 45 and 56%). The EC_a response was capable of detecting changes across landscapes and intact gilgai patterns as well, providing useful information to improve the spatial scale of information compared to NRCS soil survey maps. Because inorganic C influences the shrink-swell potential of the soil (Dinka et al.,

2013), EC_a can then be used as a proximal sensing tool to map changes in cracking potential across these landscapes. The ability to provide spatial hydrology models detailed information of soil shrink-swell potential across landscapes may help in predictions of runoff and infiltration partitioning.

CHAPTER V

SUMMARY

This research has attempted to address the spatial and temporal variability of soil crack volume associated with high shrink-swell potential with an improved measurement system, new models and proximal sensing. The benefits include advances in climate modeling, crop production modeling, reservoir management and flood warnings on shrink-swell soils due to improved predictions of runoff and infiltration.

Measuring soil shrinkage with changes in water content in a single borehole improved field shrinkage curves when compared with spatially distributed measurements. The spatially variability in a 2 m^2 area was enough to reduce the r^2 of the correlation from 0.90 to 0.73 for a 1-m soil profile. Additionally, instead of measuring soil layers between an anchor depth and the soil surface, our system measures individual soil layers. This can give a much more accurate picture of soil shrinkage with depth.

Despite this improvement in measuring soil shrinkage with water loss, models using the COLE value and soil water loss were much better at predicting soil crack volume than those using field shrinkage measurements. Using the Modified Bronswijk approximation, which is based on COLE and water loss, and photographically-estimated soil crack volume, and was highly correlated to photographically-estimated crack volume, but there was an intercept and over-predicted by a factor of 10.

Proximal sensors measuring bulk apparent electrical conductivity, like the EM38, respond to changes in inorganic C on calcareous Vertisols. Because inorganic C also

influences shrink-swell potential, it may be possible to use this information to map shrink-swell potential. This information would be helpful because many surface hydrology models are capable of fine-scale resolution, but current soil information is only available at course scales.

Future research should include validating the potential increase in macropore space as these soils dry, and the conductivity of clay films to predict how fast the soil could conduct water away from soil cracks. Additional work is also needed on crack geometry and spatial patterns, which would be used to model soil water redistribution throughout the soil profile. Implementation of this research into surface hydrology models should be pursued, and subroutines predicting the dynamic macropore space and soil crack volume using COLE and water loss should be implemented. This research provides an example of how mechanistic models using available soil data, validated with field measurements, can be successfully used to predict soil behavior.

LITERATURE CITED

Abou Najm, M., J.D. Jabro, W.M. Iversen, R.H. Mohtar, and R.G. Evans. 2010. New method for the characterization of three-dimensional preferential flow paths in the field. Water Resour. Res. 46:W02503.

Aitchison, G.D., and J.W. Holmes. 1953. Aspects of swelling in the soil profile. Aust. J. Appl. Sci. 4:244-259.

Akbar, M.A., A.L. Kenimer, and S.W. Searcy. 2004. Estimating soil profile depth with apparent electrical conductivity for a Texas Vertisol. Trans. ASAE 47:1087-1092.

Archie, G.E. 1942. The electrical resistivity log as an aid in determining some reservoir characteristics. Petrol. Trans. AIME 146:54–62.

Arnold, J.G., K.N. Potter, K.W King, and P.M. Allen. 2005. Estimation of soil cracking and the effect on surface runoff in a Texas Blackland Prairie watershed. Hydrol. Proc. 19:589-603.

Baer, J.U. and S.H. Anderson. 1997. Landscape effects on desiccation cracking in an Aqualf. Soil Sci. Soc. Am. J. 61:1497-1502.

Beven, K., and P. Germann. 1982. Macropores and water flow in soils. Water Resour. Res. 18:1311-1325.

Bouma, J., and L.W. Dekker. 1978. A case study on infiltration into dry clay soil I. morphological observations. Geoderma 20:27-40.

Brevik, E.C., T.E. Fenton and A. Lazari. 2006. Soil electrical conductivity as a function of soil water content and implications for soil mapping. Prec. Agric. 7:393-404.

Bronswijk, J.J.B. 1989. Prediction of actual cracking and subsidence in clay soils. Soil Sci. 148:87-93.

Bronswijk, J.J.B. 1990. Shrinkage geometry of a heavy clay soil at various stresses. Soil Sci. Soc. Am. J. 54:1500-1502.

Bronswijk, J.J.B. 1991. Relation between vertical soil movements and water-content changes in cracking clays. Soil Sci. Soc. Am. J. 55:1220-1226.

Cabidoche, Y.M. and M. Voltz. 1995. Non-uniform volume and water content changes in swelling clay soil: II. a field study on a Vertisol. Euro. J. Soil Sci. 46:345-355.

Cabidoche, Y-M. and S. Ruy. 2001. Field shrinkage curves of a swelling clay soil: analysis of multiple structural swellings and shrinkage phases in the prisms of a Vertisol. Aust. J. Soil Res. 39:143-160.

Cambardella, C. A., T. B. Moorman, J. M. Novak, T. B. Parkin, D. L. Karlen, R. F. Turco, and A. E. Konopka. 2001. Field-scale variability of soil properties in Central Iowa soils. Soil Sci. Soc. Am. J. 58:1501-1511.

Carroll, Z.L., M.A. Oliver. 2005. Exploring the spatial relations between soil physical properties and apparent electrical conductivity. Geoderma 128:354–374.

Chertkov, V.Y. 2007. The reference shrinkage curve of clay soil. Theor. App. Frac. Mech. 48:50-67.

Chertkov, V.Y., I. Ravina, and V. Zadoenko. 2004. An approach for estimating the shrinkage geometry factor at moisture content. Soil Sci. Soc. Am. J. 68:1807-1817.

Coquet, Y., J. Touma, and P. Boivin. 1998. Comparison of soil linear shrinkage curve from extracted cores and in situ. Aust. J. Soil Res. 36:765-781.

Corwin, D. L., and S. M. Lesch. 2005. Apparent soil electrical conductivity measurements in agriculture. Comput. Electron. Agr. 46:11-43.

Coulombe, C.E., L.P. Wilding and J.B. Dixon. 1996. Overview of Vertisols: Characteristics and impacts on society. Advances in Agronomy 57:289-375.

Crescimanno, G. and G. Provenzano. 1999. Soil shrinkage characteristic curve in clay soils: measurement and prediction. Soil Sci. Soc. Am. J. 63:25-32.

Dasog, G.S., and G.B. Shashidhara. 1993. Dimension and volume of cracks in a Vertisol under different crop covers. Soil Sci. 156:424–428.

Dinka, T.M., C.L.S. Morgan, K.J. McInnes, A.Sz. Kishne, and R.D. Harmel. 2013. Shrink-swell behavior of soil across a Vertisol catena. J. Hydrol. 475:352-359.

Doolittle, J.A., K.A. Suddduth, N.R. Kitchen, S.J. Indorante. 1994. Estimating depth to claypans using electromagnetic induction methods. J. Soil Water Conserv. 49:572-575.

Evett, S.R., J.A. Tolk, and T.A. Howell. 2003. A depth control stand for improved accuracy with the neutron probe. Vadose Zone J. 2:642-649.

Evett, S.R., J.A. Tolk, and T.A. Howell. 2006. Soil profile water content determination: Sensor accuracy, axial response, calibration, temperature dependence, and precision. Vadose Zone J. 5:894-907.

Favre, F., P. Boivin, and M.C.S. Wopereis. 1997. Water movement and soil swelling in a dry, cracked Vertisol. Geoderma 78:113-123.

Franzmeier, D.P., and S.J. Ross. 1968. Soil swelling: Laboratory measurement and relation to other soil properties. Soil Sci. Soc. Am. J. 32:573-577.

Grant, D.R. 1975. Measurement of soil moisture near the surface using a neutron moisture meter. Soil Sci. 26:124-129.

Gray, C.W., and R. Allbrook. 2002. Relationships between shrinkage indices and soil properties in some New Zealand soils. Geoderma 108:287-299.

Griffith, G., S. Bryce, J. Omernik, and A. Rogers. 2007. Ecoregions of Texas. Texas Commission on Environmental Quality. http://www.tceq.state.tx.us/assets/public/comm_exec/pubs/as/199.pdf (Accessed 18 Feb. 2014).

Haines, W.B. 1923. The volume-changes associated with variations of water content in soil. J. Agric. Sci. 13:296-264.

Hallaire, V. 1987. Vertical shrinkage of a clayey soil drying: measurements of the sinking and structural consequences. Agronomie 8:631-637.

Harmel, R.D., C.W. Richardson, K.W. King, P.M. Allen. 2006. Runoff and soil loss relationships for the Texas Blackland Prairies ecoregion. J. Hydrol. 331:471-483.

Harvey, O.R., and C.L.S. Morgan. 2009. Predicting regional-scale soil variability using a single calibrated apparent soil electrical conductivity model. Soil Sci. Soc. Am. J. 73:164-169.

Jarvis, N.J. and P.B. Leeds-Harrison. 1987. Some problems associated with the use of the neutron probe in swelling/shrinking clay soils. J. Soil Sci. 38:149-156.

Jenny, H. 1946. Arrangement of soil series and types according to functions of soil-forming factors. Soil Sci. 61:375-391.

Johnson, C.K., J.W. Doran, H.R. Duke, B.J. Wienhold, K.M. Eskridge, and J.F. Shanahan. 2001. Field-scale electrical conductivity mapping for delineating soil condition. Soil Sci. Soc. Am. J. 65:1829:1837.

Johnston, J.R. and H.O. Hill. 1945. A study of the shrinkage and swelling properties of Rendzina soils. Soil Sci. Soc. Am. J. 9:24-29.

Kachanoski, R.G., E. DeJong, I.J. van Wesenbeeck. 1990. Field scale patterns of soil-water storage from non-contacting measurements of bulk electrical conductivity. Can. J. Soil Sci. 70:537-542.

Kilmer, V.H., and L.Z. Alexander. 1949. Methods for making mechanical analyses of soil. Soil Sci. 68:15-24.

Kirby, J.M., A.L. Bernard, A.J. Ringrose-Voase, R. Young and H. Rose. 2003. Field swelling, shrinking, and water content change in a heavy clay soil. Aust. J. Soil Res. 41:963-978.

Kishne, A.Sz., C.L.S. Morgan, and W.L. Miller. 2009. Vertisol crack extent associated with gilgai and soil moisture in the Texas Gulf Coast Prairie. Soil Sci. Soc. Am. J. 73:1221-1230.

Kuhn, J., A. Brenning, M. Wehrhan, S. Koszinski, and M. Sommer. 2009. Interpretation of electrical conductivity patterns by soil properties and geological maps for precision agriculture. Precision Agric. 10:490-507.

Lepore, B.J., C.L.S. Morgan, J.M. Norman, and C.C. Molling. 2009. A mesopore and matrix infiltration model base on soil structure. Geoderma 152:301-313.

Lund, E.D., D. Christy, and P.E. Drummond. 1999. Applying soil electrical conductivity technology to precision agriculture. In: P.C. Robert, R.H. Rust, and W.E. Larson, editors, Proceedings of the 4th International Conference on Precision Agriculture. ASA: Madison, WI. p. 1089–1100.

Mbagwu, J.S.C., and O.G. Abeh. 1998. Prediction of engineering properties of tropical soils using intrinsic pedological properties. Soil Sci. 163:93-102.

McBratney, A.B., B. Minasny, and B.M. Whelan. 2005. Obtaining 'useful' high – resolution soil data from proximally-sensed electrical conductivity/resistivity (PSEC/R) surveys. Precision Ag. 503:510.

McBratney, A.B., B. Minasny, S.R. Cattle, and R.W. Vervoort. 2002. From pedotransfer functions to soil inference systems. Geoderma 109:41-73.

McBratney, A.B., M.L.M. Santos, and B. Minasny. 2003. On digital soil mapping. Geoderma 117:3-52.

McBride, R.A., A.M. Gordon, S.C. Shrive. 1990. Estimating forest soil quality from terrain measurements of apparent electrical conductivity. Soil Sci. Soc. Am. J. 54:290-293.

McIntyre, D.S., C.L. Watson, and J. Loveday. 1982. Swelling of a clay soil profile under ponding. Aust. J. Soil Res. 20:71-79.

McNeil, J.D. 1980. Electromagnetic terrain conductivity measurement at low induction numbers. Tech Note TN5. Geonics, LTD., Mississauga, Ontario, Canada. http://www.georentals.co.uk/tn6.pdf (Accessed 4 March 2014).

Miller, W.L., A.Sz. Kishne, and C.L.S. Morgan. 2010. Vertisol morphology, classification, and seasonal cracking patterns in the Texas Gulf Coast Prairie. Soil Surv. Horiz. 51:10-16.

Mitchell, A.R. and M.Th. van Genuchten. 1992. Shrinkage of bare and cultivated soil. Soil Sci. Soc. Am. J. 56:1036-1042.

National Cooperative Soil Survey. National Cooperative Soil Characterization Database. Available online at http://ncsslabdatamart.sc.egov.usda.gov (Accessed 7 Jan. 2014).

Paton, T.R. 1974. Origin and terminology for gilgai in Australia. Geoderma 11:221-242.

Rhoades, J.D. 1982. Cation exchange capacity. In: A.L. Page, R.H. Miller, and D.R. Keeney, editors, Methods of soil analysis. Part 2. Agron. Monogr. 9, ASA, Madison, WI. p. 149-157.

Rhoades, J.D., D.L. Corwin, 1981. Determining soil electrical conductivity-depth relations using inductive electromagnetic soil conductivity meter. Soil Sci. Soc. Am. J. 45:255–260.

Rhoades, J.D., P.A.C. Raats, and R.S. Prather. 1976. Effects of liquid-phase electrical conductivity water content and surface conductivity on bulk soil electrical conductivity. Soil Sci. Soc. Am. J. 40:651-665.

Rivera, L.D. 2011. Comparing methods of estimating crack volume in shrink-swell soils. Thesis, Texas A&M University. Available electronically from http://repository.tamu.edu/handle/1969.1/98359.

Robinson, N. J., Rampant, P. C., Callinan, A. P. L., Rab, M. A., Fisher, P. D. 2009. Advances in precision agriculture in south-eastern Australia. I. Spatio-temporal prediction of crop yield using terrain derivatives and proximally sensed data. Crop Pasture Sci. 60, 859–869.

Schelling, J. 1970. Soil genesis, soil classification and soil survey. Geoderma. 4:165-193.

Serrano, J.M., J.O. Peca, J.R. Marques da Silva, and D. Shaidian. 2010. Mapping soil and pasture variability with an electromagnetic induction sensor. Comput. Electron. Agric. 73:7-16.

Sheets, K.R. and J.M.H. Hendricx. 1995. Noninvasive soil water content measurement using electromagnetic induction. Water Resour. Res. 31:2401-2409.

Sherrod, L.A., G. Dunn, G.A. Peterson, and R.L. Kolberg. 2002. Inorganic carbon analysis by modified pressure-calcimeter method. Soil. Sci. Soc. Am. J. 66:299-305.

Smith, C.W., A. Hadas, J. Dan, and H. Koyumdjisky. 1985. Shrinkage and Atterberg limits in relation to other properties of principal soil types in Israel. Geoderma 35:47-65.

Soil Survey Staff. 2014. Natural Resources Conservation Service, United States Department of Agriculture. Web Soil Survey. Available online at http://websoilsurvey.nrcs.usda.gov/. (Accessed 4 March 2014).

Stewart, R.D., M.R. Abou Najm, D.E. Rupp, and J.S. Selker. 2012. Measurement tool for dynamics of soil cracks. Vadose Zone J. 11:-.

Stirk, G.B. 1954. Some aspects of soil shrinkage and the effect of cracking upon water entry into the soil. Austr. J. Agr. Res. 5:279-290.

Tempany, H.A. 1917. The shrinkage of soil. J. Agric. Sci. 8:312-330.

Towner, G.D. 1968. Variability of soil moisture in the black cracking clay soil of north-western New South Wales. Aust. J. Exp. Agric. Anim. Husb. 8:252-254.

van der Klooster, E., F.M. van Egmond, and M.P. Sonneveld. 2011. Mapping soil clay contents in Dutch marine districts using gamma-ray spectrometry. Euro. J. Soil Sci. 62:743-753.

Weller, U., M. Zipprich, M. Sommer, W.Zu. Castell, and M. Wehrhan. 2007. Mapping clay content across boundaries at the landscape scale with electromagnetic induction. Soil Sci. Soc. Am. J. 71:1740-1747.

Western, A. and G. Bloschl. 1999. On the spatial scaling of soil moisture. J. Hydrol. 217:203-224.

Wilding, L.P., and D. Tessier. 1988. Genesis of Vertisols: Shrink-swell phenomena. In L.P. Wilding and R. Puentes, editors, Vertisols: their distribution, properties, classification and management. USDA Soil Management Support Services, Tech. Monogr. 18. Texas A&M Univ. Printing Center, College Station, TX. p. 55-81.

Wilding, L.P., D. Williams, W. Miller, T. Cook, and H. Eswaran. 1989. Close interval spatial variability of Vertisols: a case study in Texas. In J.M. Kimble, editor, Proc. 6th Int. Soil Correlation Meeting (VI ISCOM), Characterization, Classification and Utilization of Cold Aridisols and Vertisols, Aug. 6–18, 1989. USDA Soil Conservation Service, National Soil Survey Center, Lincoln, NE. p. 232–247.

Wilke, K.A. 2010. Using visible and near infrared diffuse reflectance spectroscopy to characterize and classify soil profiles. Thesis, Texas A&M University. Available electronically from http://repository.tamu.edu/handle/1969.1/ETD-TAMU-2010-08-8213.

Woodruff, C.M. 1937. Linear changes in the Shelby loam profile as a function of soil moisture. Soil Sci. Soc. Am. J. 1:65:70.

Yule, D.F., and J.T. Ritchie. 1980. Soil shrinkage relationships of Texas Vertisols: I. small cores. Soil Sci. Am. J. 44:1285-1291.

Zhu, Q., H.S. Lin, and J.A. Doolittle. 2010a. Repeated electromagnetic induction surveys for determining subsurface hydrologic dynamics in an agricultural landscape. Soil Sci. Soc. Am. J. 74:1750–1762.

Zhu, Q., H.S. Lin, and J.A. Doolittle. 2010b. Repeated electromagnetic induction surveys for improved soil mapping in an agricultural landscape. Soil Sci. Soc. Am. J. 74:1763–1774.